NASA CONTRACTOR REPORT

A CONTRIBUTION TO THE MICROMECHANICS OF COMPOSITE MATERIALS - STRESSES AND FAILURE MECHANISMS INDUCED BY INCLUSIONS

by H. Schuerch

Prepared by
ASTRO RESEARCH CORPORATION
Santa Barbara, Calif.
for Western Operations Office

NATIONAL AERONAUTICS AND SPACE ADMINISTRATION • WASHINGTON, D. C. • SEPTEMBER 1966

NASA CR-582

A CONTRIBUTION TO THE MICROMECHANICS OF COMPOSITE MATERIALS - STRESSES AND FAILURE MECHANISMS INDUCED BY INCLUSIONS

By H. Schuerch

Prepared under Contract No. NAS 7-427 by
ASTRO RESEARCH CORPORATION
Santa Barbara, Calif.

for Western Operations Office

NATIONAL AERONAUTICS AND SPACE ADMINISTRATION

For sale by the Clearinghouse for Federal Scientific and Technical Information
Springfield, Virginia 22151 – Price $2.50

ACKNOWLEDGEMENT

The development of the closed form solutions for the stress functions and mapping of data was performed by W. Robbins and P. Preiswerk. The graphical representation of stress surfaces and contour maps is due to C. Olcott.

The work resulting in this report has been conducted with the financial assistance of the National Aeronautics and Space Administration.

TABLE OF CONTENTS

LIST OF SYMBOLS

a	(in)	=	radius of circular inclusion
A,B,C,D		=	integration constants
E	(psi)	=	Young's modulus
F^2	$(psi)^2$	=	Hencky-v. Mises distortion energy failure criterion
K_1 K_2		=	non-dimensional elastic composite constants
r	(in)	=	radial coordinate
s	(psi)	=	applied stress
z	(in)	=	axial coordinate
δ		=	angle between principal stress and radial direction
μ		=	Poisson's ratio
Φ		=	Airy stress function
σ	(psi)	=	normal stress
θ		=	azimuth coordinate angle
τ	(psi)	=	shear stress

Subscripts

f	=	refers to inclusion
m	=	refers to matrix
r	=	radial stress component
$1, 2, 3$	=	refers to principal stresses
θ	=	tangential stress component

LIST OF FIGURES

LIST OF FIGURES

LIST OF FIGURES

SUMMARY

Stress function methods are used to determine the field of stress concentrations produced by cylindrical inclusions in an otherwise homogeneous matrix material subject to an applied stress transverse to the inclusion axis. It is found that the stress field generated by single cylindrical inclusions can be completely characterized by two non-dimensional constants that depend upon the relative elastic properties of the composite. Additional results are given for the case of an inclusion in the form of a spherical void.

The stress field is presented graphically in the form of stress surfaces for a number of selected cases. The calculated stress fields are interpreted in terms of fracture mechanics for non-ideally loaded fiber composites, and for several types of polycrystalline ceramics.

Based upon the analytical studies, guidelines are developed for composites using advanced types of microgeometry. Several promising approaches are reduced to the fabrication of laboratory test specimens.

INTRODUCTION

The useful "design strength" of high performance filamentary composite materials is frequently disappointingly low because, in practical applications, stresses in directions other than along the fiber axis are incurred. Such non-ideal loadings may involve normal stresses applied in directions transverse to the fiber axis, such as in the case of biaxially stressed, cross-laminated shells, pressure vessels, etc. Similar conditions occur due to geodesic fiber curvature, non-columnated fibers, or due to conditions prevailing at points of concentrated loadings, attachments or individually discontinuous fibers.

In some instances, these non-ideal applications are avoidable by appropriate design techniques. In many others, however, ideal design configurations need to be compromised for practical reasons, and the subject of the materials sensitivity to non-ideal loading becomes an appropriate matter of concern. Hence, the question of stress concentrations generated by the presence of inclusions in an otherwise homogeneous "matrix" body is of central interest to the mechanical functioning and failure mechanisms of composite materials, made with either ductile or non-ductile matrix materials. In addition, the nature of the stress pattern caused by inclusions

of either high or low rigidity can conceivably shed light upon the strength and failure phenomena of polyphase, non-ductile materials, such as dense or porous polycrystalline ceramics, or glassy materials with included flaws in the form of voids, or hard crystallites. Finally, a thorough understanding of geometrical microdesign effects upon fracture origin in synthetically textured materials provides guides for the development of improved composites, particularly with regard to their sensitivity to non-ideal loading conditions.

I. ANALYSIS OF STRESSES DUE TO CIRCULAR INCLUSIONS

To obtain a detailed and quantitative insight into the stresses prevailing in the vicinity of an inclusion, the case of cylindrical inclusion with a circular section embedded in an infinite slab of otherwise homogeneous matrix material, subject to uniaxial stress, has been analyzed (Fig. 1). Assuming Hookean materials, this problem lends itself to a rigorous closed form solution for the two limiting cases of plane stress and plane strain. The results of this analysis may also be considered as a first approximation for multiple inclusions, spaced several diameters from each other, rendering the mutual influence of adjacent inclusions relatively unimportant or allowing reasonable approximations by superposition of interfering stress patterns. The closed form solutions, furthermore, can aid in the development of digital computer programs which are capable of handling arbitrary geometrical arrays of inclusions, by providing checks for accuracy and formulations for initial conditions.

Considering the symmetry of the problem shown in Figure 1, the Airy stress function satisfying the biharmonic differential equation in polar coordinates is: (Ref. 1)

$$\Phi = A_o \log_e r + B_o r^2 \log_e r + C_o r^2 + \sum_{n=1}^{\infty} \left(A_{2n} r^{2n} + B_{2n} r^{2n+2} + C_{2n} r^{-2n} + D_{2n} r^{-2n+2} \right) \cos 2n\theta \qquad (1)$$

Since the stress remains finite for $r \to \infty$, the coefficient B_o has to be zero. Only the first term (n=1) of the Fourier series needs to be used. Thus the stress function reduces to

$$\Phi = A_o \log_e r + C_o r^2 + \left[A_2 r^2 + B_2 r^4 + C_2 \frac{1}{r^2} + D_2 \right] \cos 2\theta \tag{1a}$$

and the stresses are obtained from the derivatives as follows:

$$\left.\begin{aligned} \sigma_r &= \frac{1}{r}\frac{\partial \Phi}{\partial r} + \frac{1}{r^2}\frac{\partial^2 \Phi}{\partial \theta^2} = \frac{A_o}{r^2} + 2C_o - \left[2A_2 + 6C_2 \frac{1}{r^4} + 4D_2 \frac{1}{r^2} \right] \cos 2\theta \\ \sigma_\theta &= \frac{\partial^2 \Phi}{\partial r^2} = -\frac{A_o}{r^2} + 2C_o + \left[2A_2 + 12B_2 r^2 + 6C_2 \frac{1}{r^4} \right] \cos 2\theta \\ \tau_{r\theta} &= -\frac{\partial}{\partial r}\left(\frac{1}{r}\frac{\partial \Phi}{\partial \theta} \right) = \left[2A_2 + 6B_2 r^2 - 6C_2 \frac{1}{r^4} - 2D_2 \frac{1}{r^2} \right] \sin 2\theta \end{aligned}\right\} \tag{2}$$

Both sets of six coefficients A_o, C_o, A_2, B_2, C_2, D_2, for the inclusion and the matrix can be determined by boundary

conditions. After some algebraical transformations, it can be shown that the solutions can be expressed in terms of two groupings, K_1, and K_2, of the relative elastic properties of matrix and inclusion, where:

for plane stress:	for plane strain:
$K_1 = \frac{E_f(1-\mu_m) - E_m(1-\mu_f)}{E_f(1+\mu_m) + E_m(1-\mu_f)}$;	$K_1 = \frac{E_f(1-2\mu_m)(1+\mu_m) - E_m(1-2\mu_f)(1+\mu_f)}{E_f(1+\mu_m) + E_m(1-2\mu_f)(1+\mu_f)}$
$K_2 = \frac{E_f(1+\mu_m) - E_m(1+\mu_f)}{E_f(3-\mu_m) + E_m(1+\mu_f)}$;	$K_2 = \frac{E_f(1+\mu_m) - E_m(1+\mu_f)}{E_f(3-4\mu_m)(1+\mu_m) + E_m(1+\mu_f)}$

and where E is the Young's modulus, μ is the Poisson's ratio; the subscript f refers to the inclusion, and the subscript m refers to the matrix. With these factors, the stress distribution (2) reduces to two sets of expressions:

inside the inclusion ($r < a$):

$$\frac{\sigma_r}{s} = \frac{1}{2}(1+K_1) + \frac{1}{2}(1+K_2)\cos 2\theta$$

$$\frac{\sigma_\theta}{s} = \frac{1}{2}(1+K_1) - \frac{1}{2}(1+K_2)\cos 2\theta \qquad (2a)$$

$$\frac{\tau_{r\theta}}{s} = -\frac{1}{2}(1+K_2)\sin 2\theta$$

$$\frac{\sigma_z}{s}^{*)} = \mu_f (1+K_1)$$

and in the matrix ($r > a$)

$$\frac{\sigma_r}{s} = \frac{1}{2}\left(1+K_1 \frac{a^2}{r^2}\right) + \frac{1}{2}\left[1-K_2\left(3\frac{a^4}{r^4} - 4\frac{a^2}{r^2}\right)\right]\cos 2\theta$$

$$\frac{\sigma_\theta}{s} = \frac{1}{2}\left(1-K_1 \frac{a^2}{r^2}\right) - \frac{1}{2}\left[\left(1-3K_2 \frac{a^4}{r^4}\right)\right]\cos 2\theta \qquad (2b)$$

$$\frac{\tau_{r\theta}}{s} = -\frac{1}{2}\left[1 + K_2\left(3\frac{a^4}{r^4} - 2\frac{a^2}{r^2}\right)\right]\sin 2\theta$$

$$\frac{\sigma_z}{s}^{*)} = \mu_m\left(1 + 2K_2\frac{a^2}{r^2}\cos 2\theta\right)$$

*) Only for plane strain

Hence, the stress field is completely characterized by the two non-dimensional composite elastic constants K_1, and K_2, which in turn, are unique functions of the modulus ratio, the Poisson's ratios of both constituents, and the assumptions regarding the third principal stress (or strain). This reduction of parameters aids considerably in the detailed evaluation of stress fields.

The corresponding principal stresses to the stress distribution given in Eqns. (2a) and (2b) are obtained by the well-known transformations:

$$\sigma_{1,2} = \frac{1}{2}(\sigma_r + \sigma_\theta) \pm \frac{1}{2}\left[\left(\sigma_r - \sigma_\theta\right)^2 + 4\,\tau_{r\theta}^2\right]^{1/2}$$

and the angle δ between the direction of the principal stress (stress trajectory), and the radial direction is obtained from

$$\tan 2\delta = \frac{2\tau_{r\theta}}{\sigma_r - \sigma_\theta}$$

With these transformations, the principal stress magnitudes and trajectory angles inside the inclusion ($r < a$) become:

$$\left.\begin{aligned} \frac{\sigma_1}{s} &= 1 + \frac{1}{2}(K_1 + K_2) \\ \frac{\sigma_2}{s} &= \frac{1}{2}(K_1 - K_2) \\ \delta &= -\theta \end{aligned}\right\} \qquad (3a)$$

Hence the stress distribution inside the inclusion is uniform but biaxial, the principal axes being aligned parallel and normal to the axis of applied stress. In view of the very complicated stress field in the matrix surrounding the inclusion, this result is, at first sight, quite surprising. It should also be observed that this result holds for multiple inclusions only if these are widely spaced.

The principal stresses and their trajectory angle in the matrix are obtained from (2b):

$$\left.\begin{aligned}
\frac{\sigma_1}{s} &= \frac{1}{2}\left\{ 1 + \frac{a^2}{r^2}\left(2K_2 \cos 2\theta + K_1 \cos 2\delta \right) + \right. \\
&+ \left. \left[1-K_2\left(3\frac{a^4}{r^4} - 2\frac{a^2}{r^2}\right)\right]\cos 2\theta \cos 2\delta - \left[1+K_2\left(3\frac{a^4}{r^4} - 2\frac{a^2}{r^2}\right)\right]\sin 2\theta \sin 2\delta \right\} \\
\frac{\sigma_2}{s} &= \frac{1}{2}\left\{ 1 + \frac{a^2}{r^2}\left(2K_2 \cos 2\theta - K_1 \cos 2\delta \right) - \right. \\
&- \left. \left[1-K_2\left(3\frac{a^4}{r^4} - 2\frac{a^2}{r^2}\right)\right]\cos 2\theta \cos 2\delta + \left[1+K_2\left(3\frac{a^4}{r^4} - 2\frac{a^2}{r^2}\right)\right]\sin 2\theta \sin 2\delta \right\} \\
\tan 2\delta &= -\frac{\left(1 + K_2\left[3\frac{a^4}{r^4} - 2\frac{a^2}{r^2}\right]\right)\sin 2\theta}{\left(1 - K_2\left[3\frac{a^4}{r^4} - 2\frac{a^2}{r^2}\right]\right)\cos 2\theta + K_1\frac{a^2}{r^2}}
\end{aligned}\right\} \quad (3b)$$

Finally, for the investigation of failure in ductile components of the composite, the distortion energy, F^2, (Hencky - v. Mises, Ref. 2) is of interest:

$$F^2 = \frac{1}{2} (\sigma_1 - \sigma_2)^2 + (\sigma_2 - \sigma_3)^2 + (\sigma_3 - \sigma_1)^2 \qquad (4)$$

This expression becomes for plane stress

$$F^2 = \sigma_1^2 + \sigma_2^2 - \sigma_1 \sigma_2 \qquad (4a)$$

and for plane strain

$$F^2 = (\sigma_1^2 + \sigma_2^2)(1-\mu+\mu^2) - \sigma_1 \sigma_2 (1+2\mu-2\mu^2)$$

or

$$F^2 = 4 \tau_{max}^2 + \sigma_1 \sigma_2$$

II. EVALUATION OF SOLUTIONS

A. Stresses Inside Inclusion

As seen from Equation (3a), the stress condition inside the inclusion is uniform, biaxial for plane stress and triaxial for plane strain. The principal stress trajectories, therefore, form a rectangular pattern as shown in Figure 2. Also shown in Figure 2 are the values for the stress concentration factors σ/s in function of the modulus ratio, E_f/E_m, for two typical combinations of Poisson's ratio, and for conditions of either plane stress or plane strain.

It will be observed that rigid inclusions act as stress concentrators, experiencing a direct principal stress of approximately 1.5 times the stress applied far away from the inclusion. Stress reversal is observed, amounting to values as high as -.5. The existence of stress reversal is significant for cases where tensile fracture can originate within the inclusion due to an applied compressive stress. This may occur, particularly in the case of fibers with present or incipient longitudinal cracks, such as observed, for instance, in composite boron fibers (Refs. 3, 4).

B. Stresses in Matrix

While the condition of stress in the inclusion is uniform, the stress in the matrix in the vicinity of the inclusion is quite complex.

Three limiting cases have been evaluated representing the effect of rigid inclusions, of voids and of differential Poisson's ratios.

Table I below summarizes the three cases and lists the corresponding values for K_1 and K_2 for both plane stress and plane strain conditions.

TABLE I

COMPOSITE ELASTIC CONSTANTS USED FOR EVALUATION

	Plane Stress		Plane Strain	
	K_1	K_2	K_1	K_2
Hole: $E_f/E_m = 0$	-1	-1	-1	-1
Rigid Inclusion: $E_f/E_m = \infty$ $\mu_m = .3$	.539	.4815	.4	.5556
Different Poisson's Ratios $E_f/E_m = 1$ $\mu_f = 0$; $\mu_m = .5$	-.2	.1492	-.40	.20

The stress field for these three cases has been completely evaluated. A difficulty arises in the visual presentation of the stress tensor which is required to develop an intuitive insight into the micromechanical aspects of the stress field and its implications upon choice of improved geometries. For this reason, a somewhat unconventional presentation in the form of two principal stress surfaces with parametric lines representing the principal stress trajectories has been chosen. Hence, the results are mapped in the form of two "stress surfaces" for σ_1 and σ_2, and their associated stress trajectories in Figure 3 for a cylindrical void, Figures 4 and 5 for the rigid inclusion, and Figures 6 and 7 for a cylindrical inclusion of equal modulus but different Poisson's ratio. The vertical distance between the σ_1 and σ_2 surfaces is a measure for twice the principal shear stress, 2τ. Also shown are the lines of uniaxial stress, i.e., the loci where one of the principal stresses vanishes. The data are also presented in the more conventional form of contour maps for the principal stresses, and for the Hencky-v. Mises distortion energy in Figures 8-13.

For the purpose of comparison, and for the purpose of assessing the cascading effect discussed in Section III, the case of a spherical void has also been evaluated.

It is assumed that a homogeneous matrix is subject to a uniform uniaxial applied stress at a great distance from the spherical void. The evaluation is based upon

the solutions given by Southwell and Gough (Ref. 5). Results are presented for the meridional plane in the form of contour maps for the three principal stresses in Figure 14, and in Figure 15 in the form of the radial stress distribution for the rotationally symmetrical pattern in the equatorial plane of the spherical void.

The case for the rigid inclusion with plane stress assumption (Fig. 4) shows an interesting singularity in the form of a point of biaxial isotropic stress, located a very short distance (i.e., about .4% of the fiber radius) outside the inclusion interface. At this point, a discontinuity of stress trajectories occurs. A detail of this singularity is shown in Figure 16. A similar point is observed at the surface of the void (Fig. 3), where both principal stresses vanish.

The stress singularity for the rigid inclusion is of interest because it is located within a distance from the fiber which may be sufficiently small to be affected by the discrete nature of the molecular structure of the matrix material. For a conventional glass fiber with a radius of 2μ, for instance, the distance between surface and stress singularity is only 80Å, which is well within the size range of polymeric molecules.

The presence of both direct and reverse stress concentration factors is observed - i.e., the presence of the inclusion

causes the stress to be magnified and also to be locally reversed. Thus, for instance, application of compression to the material will cause localized areas to be subject to tension. Stress reversal peaks are also observed in the case of the cylindrical void and of the rigid inclusion in areas removed from the interface. Table II summarizes the magnitude and locations of the extremes for the principal stress and the Hencky-v. Mises distortion energies.

The effect of relative modulus upon magnitude and location of the extremes of principal stress at the inclusion interface is shown in Figures 17 and 18 for the assumption of plane strain and Poisson's ratios of .3 for both constituents. The largest principal stress is found at $\theta = 90°$, and the largest stress reversal at $\theta = 0°$, for the cases where $E_f/E_m < 1$, i.e., for the cases of "soft" inclusions. In the case where $E_f/E_m > 1$ (hard inclusions), the stress extremes occur at azimuth angles ranging from 23° to 21° for largest principal stress and at azimuth angles ranging from 54° to 62° for the largest stress reversal.

The distribution of the principal stress magnitudes, and of the stress components tangential and normal to the interface for the case of a rigid inclusion ($E_f/E_m = \infty$) are shown in Figure 19. The tangential and normal stress components may

be used for the prediction of interface failure by means of a shear-tension interaction failure hypothesis commonly employed in the strength analysis of thin bonded or brazed joints. The principal interface stresses may be used in the case where an "interface complex" exists of sufficient thickness to allow applying classical failure criteria (such as the Hencky-v. Mises or the maximum principal stress criterion).

TABLE II MAGNITUDE AND LOCATION OF EXTREME STRESS CONCENTRATION

INCLUSION	CONDITION	σ_1/s	θ	r/a	σ_2/s	θ	r/a	σ_3/s	θ	r/a	$F^2/2s$	θ	r/a
Void, $E_f/E_m = 0$	Plane Stress	3.0	90°	1.0	.375	90°	1.3				9.0	90°	1.0
$\mu_m = .3$		-.04	0°	1.1	-1.0	0°	1.0						
	Plane Strain	3.0	90°	1.0	.375	90°	1.3	.90	90°	1.0	7.11	90°	1.0
		-.04	0°	1.1	-1.0	0°	1.0	-.30	0°	1.0			
	Spherical Void	2.046	90°	1.0	.205	90°	1.3	.136	90°	1.0	7.85	90°	1.0
		-.04	0°	1.07	-.682	0°	1.0	-.682	0°	1.0			
Rigid, $E_f/E_m = \infty$	Plane Stress	1.535	21°	1.0	.45	0°	1.0				2.27	35°	1.0
$\mu_f = \mu_m = .3$		.02	90°	1.0	-.40	60°	1.0				2.02	0°	1.3
	Plane Strain	1.55	20°	1.0	.63	0°	1.0	.633	0°	1.0	2.0	40°	1.0
		1.52	0°	1.1	-.46	62°	1.0	-.033	90°	1.0	1.44	0°	1.4
Varying Poisson's Ratio	Plane Stress	1.09	35°	1.0	.315	0°	1.0				1.24	45°	1.0
$E_f/E_m = 1$		1.04	0°	1.6	-.175	72°	1.0				1.15	90°	1.5
$\mu_f = 0$	Plane Strain	1.14	35°	1.0	.50	0°	1.0	.70	0°	1.0	1.29	55°	1.0
$\mu_m = .5$		1.035	0°	1.7	-.30	90°	1.0	.30	90°	1.0	1.20	90°	1.2

III. DISCUSSION

A. Failure Mechanics of Composites

The presence of "hard" inclusions generates stress concentrations, localized primarily at the interface between inclusion and matrix. This effect is compounded by Poisson's ratio differences between matrix and inclusion. A review of the stress pattern in the surrounding matrix material (see Figures 4, 5, 10 and 11) suggests that sub-linear elastic behavior, ductile yielding, etc., of the matrix will not relieve but will rather aggravate such stress concentrations, contrary to the ductile stress relief found in the case of "soft" inclusions, notches, and voids in a strong parent material. This is due to the unfavorable "series" characteristics of the "hard" inclusion case (Fig. 20a), which attracts higher stresses into the critical interface areas as the surrounding matrix begins to weaken due to yielding. This behavior is the reverse of the "parallel" character of multiple connected domains represented by a matrix with "soft" inclusions or with included voids (Fig. 20b).

The domains of significant stress concentrations at the interface are generally small compared with the diameter of the inclusion. Thus, ductile relief of those areas will generally be limited; significant plastic flow (in metallic matrices) may be expected to predominate in areas somewhat removed from the

interface. Areas of maximum stresses and of highest distortion energy are also associated with unusually large local stress gradients. The effect of large stress gradients upon yield and fracture boundaries will require the formulation and experimental verification of appropriate criteria. This should constitute a fruitful field for future research.

In addition to the stress concentrations at the interface, hard inclusions will also be subject to internal stresses higher than the average applied stress (See Fig. 2). The stress condition internal to the inclusion, moreover, is biaxial and subject to transverse stress reversal. Thus, even in the case of lateral compression of the composite, tensile transverse stresses may occur. These can be the original cause of premature fracture, particularly in the case of brittle, hard fibers that may be subject to built-in stresses and longitudinal cracks. The same statement, of course, applies to applied transverse tension where, particularly in the case of closely packed fibers, significant tensile stresses may be generated by an unfavorable cross-sectional fiber geometry.

An interesting and somewhat unexpected side product of this investigation refers to the theory of brittle fracture in uniaxial compression: The stress reversals occurring either on

TABLE III

TECHNICAL STRENGTH OF CERAMIC MATERIALS

TECHNICAL STRENGTH	Compressive ksi	Tensile ksi	Ratio tens/compr
Dense Ceramics:			
Steatite ($2MgO \cdot Si O_2$)	80	8.5	.11
Fosterite ($2MgO \cdot Si O_2$)	85	10	.12
Zircon ($ZrO_2 \cdot Si O_2$)	100	12	.12
Titania ($Ti O_2$)	100	7.5	.075
Alumina 85%	140	20	.14
Alumina 96%	400	25	.062
	Compressive ksi	Bending ksi	Ratio bend/compr
Porous Ceramics:			
Alumina - Highly Porous	30	10	.33
Alumina - Moderately Porous	56	21	.37
Alumina - Crushable	7	2.5	.36
Magnesia	8	2	.25
Magnesium Silicate	10	5	.5

voids or on hard inclusions appear to provide a rational and, possibly, quantitative explanation for the observed ratios of tensile and compressive strengths in brittle materials. The reasoning is as follows: Assume that the brittle material will fail if a limiting principal tensile stress is exceeded. If this material contains inclusions, then the ratio of tensile to compressive applied gross stress will equal the ratio of the direct to reverse stress concentration extremes. This ratio has been plotted in Figure 21 for the case of plane strain and cylindrical inclusions in function of modulus ratio. The ranges shown in Figure 21, varying from 1/3 to 1/4 for voids and soft inclusions (porous ceramics), and from 1/16 to 1/8 for moderately hard inclusions (dense ceramics), compare well with experienced strength ratios of a wide range of technical ceramic materials. Experimental data, taken from Reference 6, are listed in Table III for the purpose of comparison.

The possibility of a "cascading" effect of progressively smaller inclusions may be suggested. Consider, for instance, the case of a hard inclusion: Chemical or metallurgical reactions between fiber and matrix (for instance, in the case of metallic matrices with refractory fibers), or solute gases in polymeric matrices will often cause the formation of microscopic voids at the interface. Thus, a situation now arises, where in addition

to the stress field generated by the hard inclusion, a "subfield" exists in the domains of the still smaller spherical voids. If these voids are located in areas of either positive or reverse stress concentrations, a multiplicative effect upon either will be observed. The magnitude of this multiplicative or "cascading" effect can be estimated from the data given in Table II. Conversely, the cascading effect may conceivably be employed to provide favorable stress field interactions by judicious choice of both relative sizes and packing geometries. Examples for this approach are discussed in the following section.

B. Guidelines for the Microdesign Development of Improved Composites

Several avenues of improving the transverse failure characteristics of fiber composites are indicated by the present analysis.

The resistance to fracture due to transverse strains can be improved by appropriate choice of cross-sectional geometry. The use of elliptical fiber sections has been suggested by Rosen, et al (Ref. 7), and experimental work on macroscopic model composites has confirmed predicted improvements in transverse modulus. In addition, an approximate analysis of the stress field in the matrix of a composite made from moderately closely packed fibers of rhombic section showed considerable promise in producing uniform stress fields and good lateral compliance by simple shearing

deformation of the matrix even for completely rigid fibers.

An analysis was conducted in predicting the transverse modulus of laminates made from fibers with rhombic sections for a range of packing densities. The results are summarized in Figure 22. Also, in Figure 22 are shown the experimental data for elliptical fiber composites and, for comparison, the theoretically available range for round fibers, based upon work published in Reference 7.

IV. EXPERIMENTAL STUDIES

A. Composite Materials With Shaped Reinforcements

Glass fibers with quasi-elliptical sections have been obtained in experimental quantities from DeBell and Richardson Inc. (Ref. 8). The cross-section of a laminate made from these fibers in an epoxy resin is shown in Figure 23. The desired nesting geometry was not fully achieved, primarily because the fiber section was oblong-rectangular with rounded edges rather than the desired elliptical section.

Due to difficulties in obtaining satisfactory solid fibers with shaped sections, this approach was abandoned in favor of a two-stage laminating process, in which shaped rods or tape is prepared in special dies from a glass-resin laminate. These elements then are subsequently bonded by an elastomeric matrix to form the final composite.

A two-stage composite material of rhombic texture (Ref. 9) was prepared to demonstrate the rhombic geometry. For this purpose, tape of flat triangular section was prepared in a shaped mandrel from standard S-glass, epoxy-impregnated roving. This tape was subjected to cure and then assembled in a rhombic pattern, using a compliant binder in the form of a high strength polyurethane elastomer.* No attempts were made to obtain optimum adhesion

* Adiprene L - Trademark: E. I. du Pont de Nemours & Co.

between the pre-cured rods and the elastomer other than normal precautions insuring reasonable cleanliness. A section of the resulting laminate is shown in Figure 24.

Another approach of utilizing microgeometrical design parameters to improve the transverse stress performance of composites is exemplified in Figure 25. Here, commercially available cylindrical rods of two diameters, made from S-glass fibers with epoxy binders, were aggregated in two typical patterns and laminated in an elastomer matrix. The pattern geometry was selected to improve packing density and, hopefully, to reduce the danger of premature transverse fracture.

An additional feature of these composites is a transverse reinforcing system, by which the individual rods were woven into a mat-like fabric shown in Figures 26 and 27. The process by which this mat is constructed is described in detail in Ref. 10. Because they are very flexible, the transverse filaments forming the cross-weave do not reduce the rod columnation, however they contribute materially to the transverse strength of the laminate. By this means, the transverse properties can be controlled to any desired degree without necessarily resorting to conventional cross-lamination. As a further advantage, the pre-fabricated mat greatly improves the ease by which practical aggregate composites of the type shown can be fabricated.

B. Test Results

It was desired to examine the relative performance of the two-stage composites described above under conditions of highly non-ideal loading. Such a test is intended to provide a measure for the materials insensitivity to "poor design", yielding a conceptual equivalent to "ductility" in conventional metallic materials.

For this purpose, test specimens representing a crude joint design have been prepared. The test specimens were mounted into a double clevis-type test fixture, as shown in Figure 28, and subject to tensile forces applied at the bolts by the test fixture. Spreading of the bolt centers was recorded in function of applied loads. The loading provided in this manner generates three types of critical stress conditions in the laminate sample:

- A transverse tensile stress in the vicinity of the bolt bearing surface that can result in catastrophic axial splitting (cleavage) of the test specimen.
- Shearing stresses along the bolt hole edge surfaces reacted by the tensile force in the specimen center that can result in progressive shear-out
- Axial compressive stresses adjacent to the bolt surface that can result in bearing failure.

The fracture appearance of five typical test specimens is shown in Figure 29. Compositions and observed mechanical properties at failure are tabulated in Table IV. Stresses at maximum bearing loads are given in two columns, one based upon total bearing area (i.e., specimen thickness times bolt diameter), and one based upon the glass fiber section in the bearing area only. Stress-displacement diagrams for the five samples are shown in Figure 30.

The maximum load at failure based upon total bearing area was generally lower in the two-stage composites than in the standard laminate. However, since the two-stage composites fail always in progressive rather than in catastrophic modes, it can be expected that careful surface preparation of the rods with primers compatible with the epoxy-glass-adiprene system would materially improve their failure load levels. Also, it will be noted that the maximum bearing stress capability based upon glass content of the two-stage composites was generally higher than that provided by the standard laminate.

The data shown in Table IV and Figure 30 indicate a major improvement in elongation at maximum load by use of the shaped rod composites as compared with the reference sample made from identical constituent materials but in the standard laminate form. The difference in failure mechanisms are also reflected

in the striking difference of failure appearance, ranging from the totally brittle, longitudinal cleavage observed in the standard laminate reference sample to progressive shear-out (Samples #1, #3, and #4), and compressive microinstability in the bearing area (Sample #3).

TABLE IV

PROPERTIES OF SHAPED TWO-STAGE COMPOSITES

#	TYPE	COMPOSITION			MECHANICAL PROPERTIES		
		Glass Vol %	Epoxy Vol %	Adiprene & Void Content Vol %	Elongation at Max. Load in	Bearing Stress at Failure Based On Total Section psi	Bearing Stress at Failure Based On Glass Section psi
1	Round Rod Aggregate 1:1 .090"/.035"	26.7	20.0	53.3	.281	4730	17,500
2	Round Rod Aggregate 1:1 090"/035"	12.8	9.6	79.6	.350	3520	27,500
3	Round Rod .035"	6.8	5.1	88.1	1.180	3700	54,400
4	Rhombic Rod 1/2" x 1/4"	61.0	20.0	19.0	.005	6860	11,200
5	Standard Laminate (Ref. Sample)	76	24	-	.002	8550	11,200

V. CONCLUSIONS

The micromechanical model subjected to analysis here represents a very much simplified version for conditions that may exist in actual cases. Evidently, for a complete characterization of the stresses prevailing in the vicinity of inclusions several other factors may have to be considered in addition to the effect of transverse stress. These include more complex applied loading patterns, non-linear materials response, stress interaction effects from neighboring inclusions, axial stress effects, and, particularly, the presence of "built-in" stresses originating, for instance, from differential thermal expansion or from interface interaction causing localized volumetric changes in the matrix-inclusion complex. The primary purpose of the work presented, therefore, is to demonstrate the utility of a rigorous analytical approach to the understanding of failure and strength in textured composite materials, rather than to yield directly applicable data for any one particular case. Nevertheless, several qualitative conclusions may be stated, based upon the foregoing results:

- The presence of hard inclusions formed by fibers in a relatively soft matrix can generate serious stress concentrations that may form the sites of origin for premature failure in actual, non-idealized structural useage of these materials.

The recognition of appropriate failure criteria provides guides towards a more judicious use of microdesign concepts, particularly with regard to the geometry of individual fibers and the packing arrangement. Significant benefits appear to be available by departing from simple round fibers of uniform diameter in more or less accidental packing arrangements. In particular, fibers with graded diameters and rhombic fiber sections in either single or two-stage composites show promise of reducing the susceptibility of potentially high strength composites to premature failure. A practical process of introducing a two or three-dimensional secondary reinforcement for control of packing geometry and improved transverse strength without degradation of the primary, unidirectional composite strength has been demonstrated in principle.

REFERENCES

1. Goodier, J. N., Timoshenko, S.: THEORY OF ELASTICITY, McGraw-Hill, 1951

2. v. Mises, R.: MECHANIK DER FESTEN KOERPER IM PLASTISCH-DEFORMABLEN ZUSTAND, Nachr. K. Ges. Wiss., Goettingen, pp 582-592, 1913

3. Witucki, R.: BORON FILAMENTS, NASA CR-96, September, 1964

4. Witucki, R.: RESEARCH ON HIGH MODULUS, HIGH STRENGTH FILAMENTS AND COMPOSITES (U), Astro Research Corporation Report ARC-R-203, November 1965 (CONFIDENTIAL)

5. Southwell, R. V., Gough, H. J.: ON CONCENTRATION OF STRESS IN THE NEIGHBORHOOD OF A SMALL SPHERICAL FLAW; AND THE PROPAGATION OF FATIGUE FRACTURES IN ELASTICALLY ISOTROPIC MATERIALS, Phil. Mag (7), pp 71-97, 1926

6. American Lava Corporation: ALSIMAG, Chart 611

7. Rosen, B. W., et al: MECHANICAL PROPERTIES OF FIBROUS COMPOSITES, NASA CR-31, April 1964

8. DeBell & Richardson, Inc.: STUDIES OF HOLLOW MULTI-PARTITIONED CERAMIC STRUCTURES", Fourth Quarterly Progress Report, June 16, 1965 - September 16, 1965.

9. U. S. Patent No. 3,121,451: ISOTENSOID STRUCTURES, February 18, 1964

10. Schuerch, H.: JOINT DESIGN FOR FLEXIBLE SPACE STRUCTURE, Paper No. VI-1, Proceedings of the Society of Aerospace Materials and Process Engineers Ninth National Symposium, Dayton, Ohio, November 1965

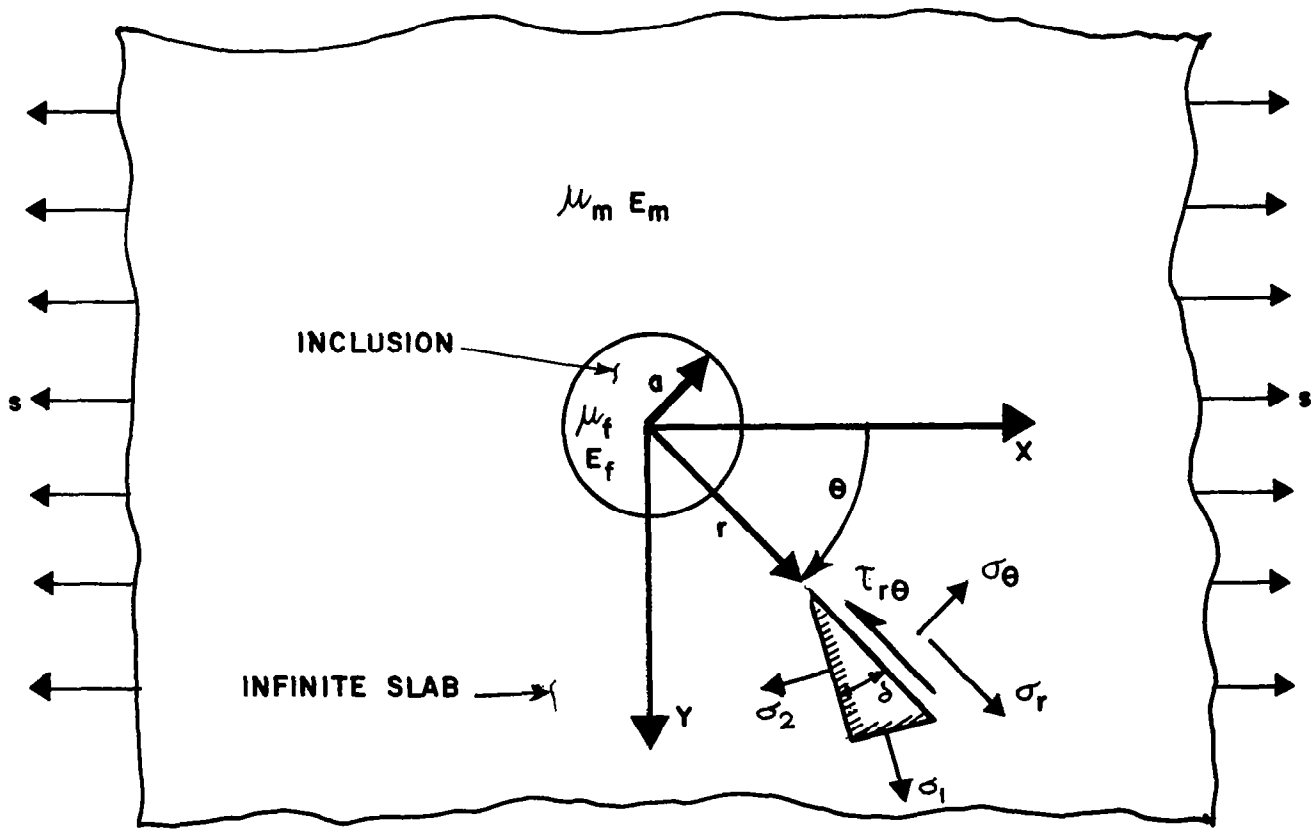

Figure 1 Infinite Body With Circular Inclusion

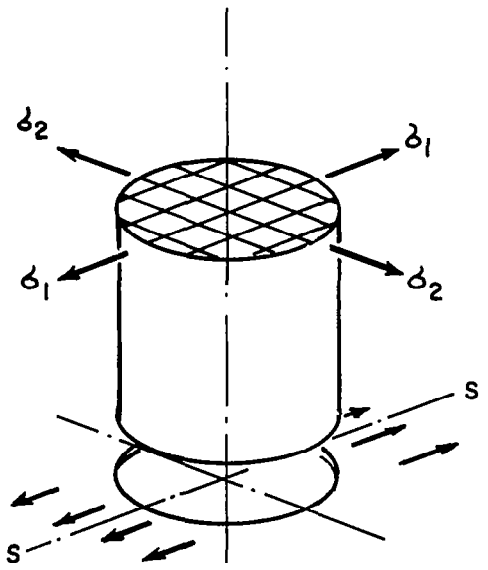

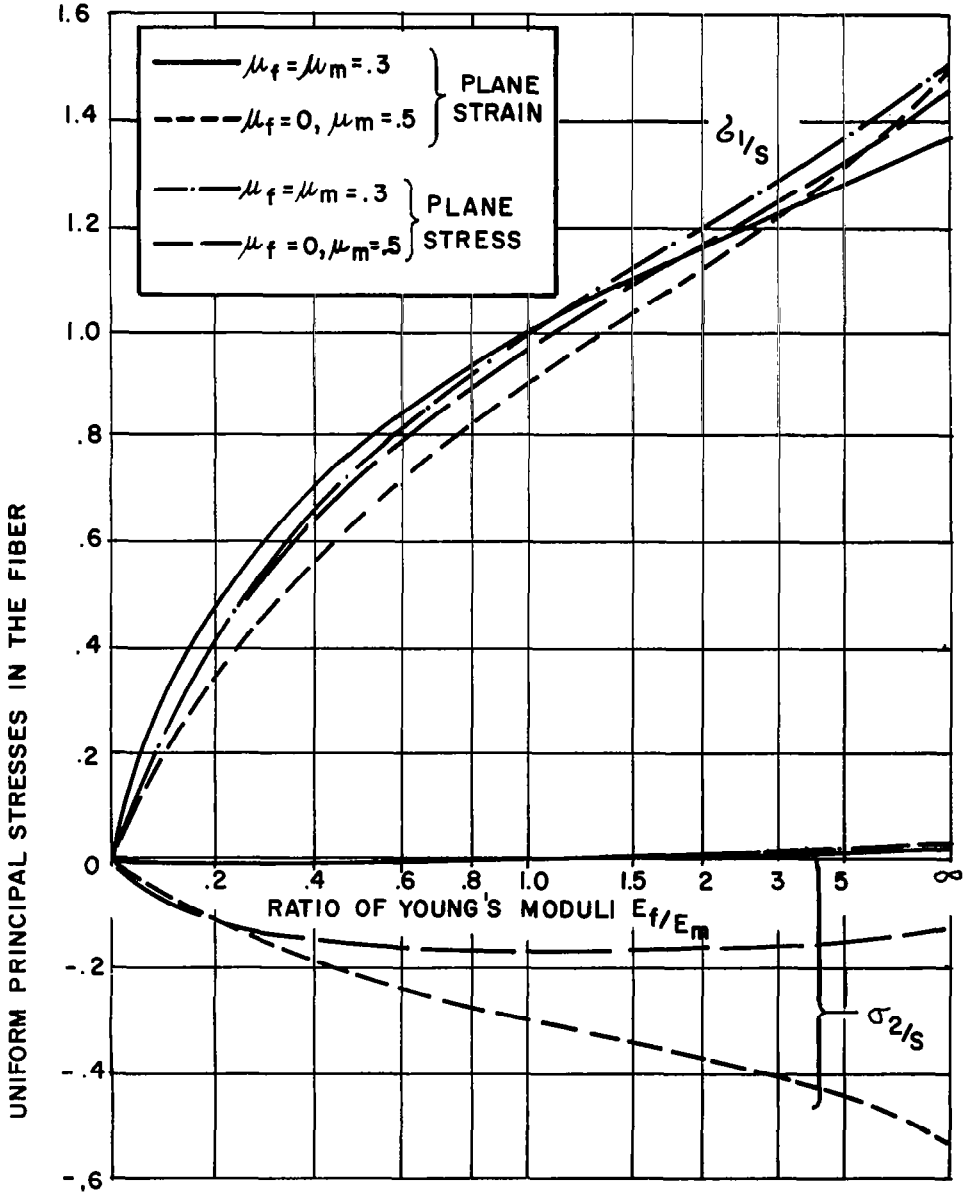

Figure 2 Stress Field Inside a Cylindrical Inclusion

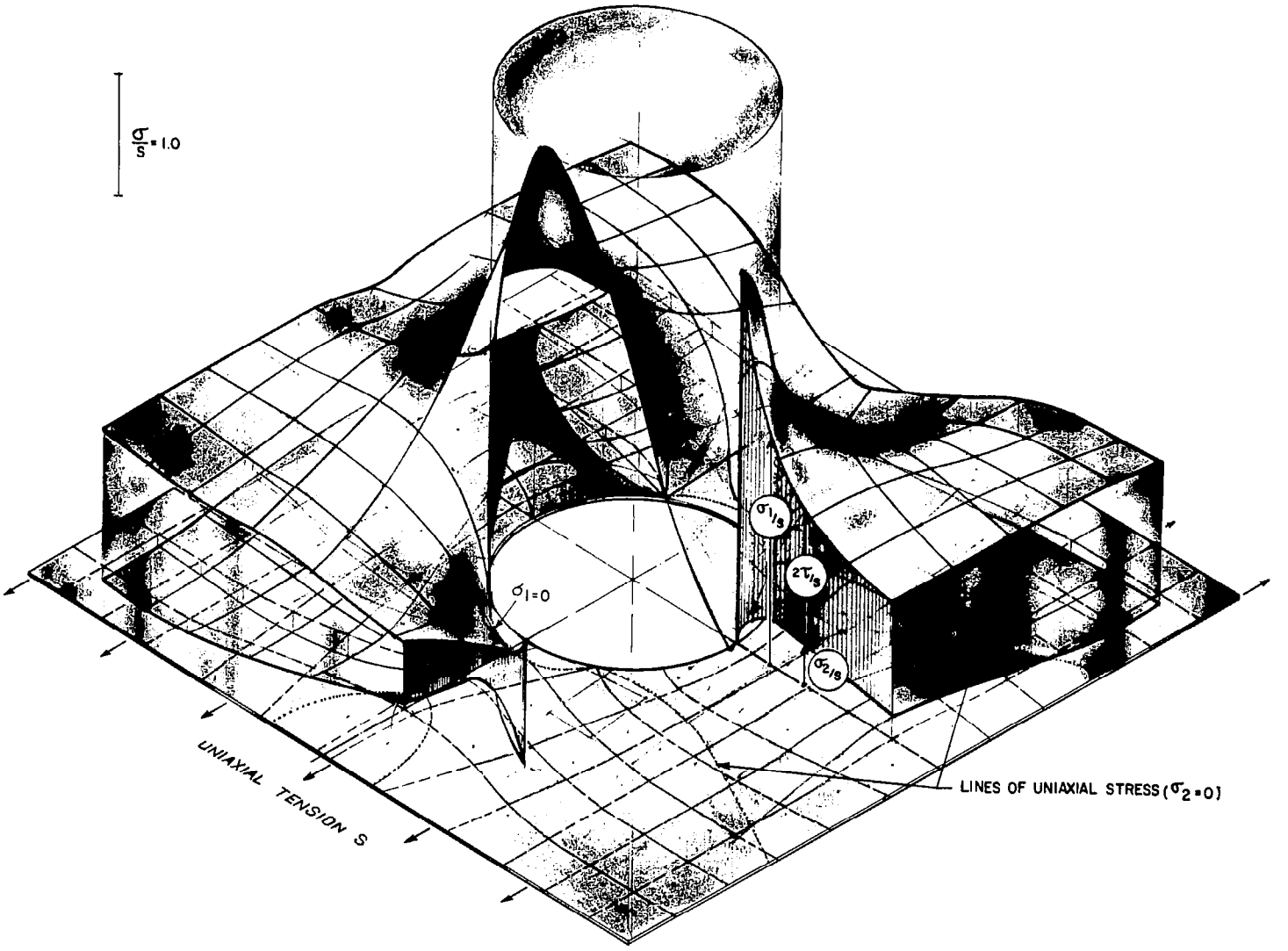

Figure 3 Stress Distribution Around A Cylindrical Void, $\mu_m = .3$

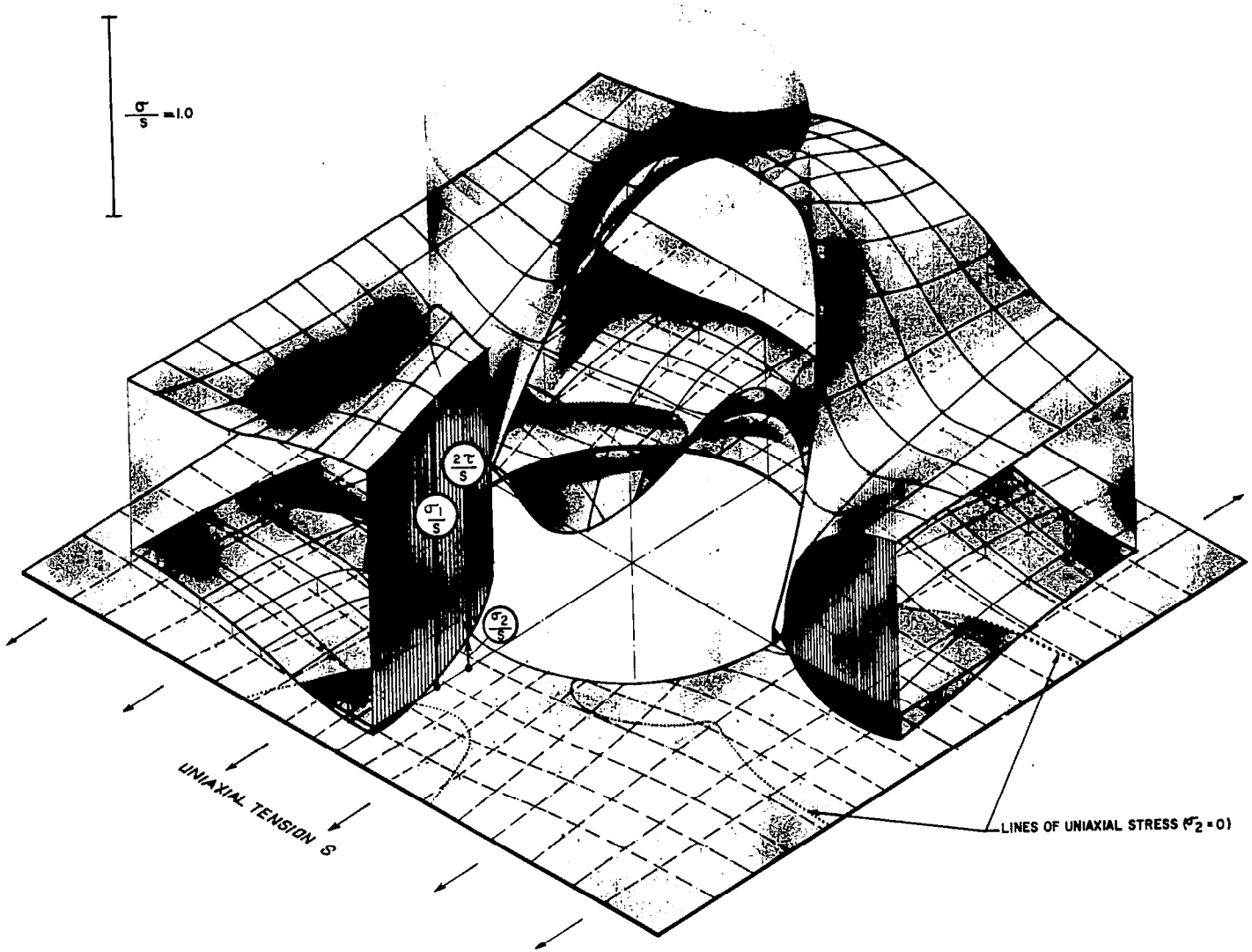

Figure 4 Stress Distribution Around A Rigid Cylindrical Inclusion (Plane Stress Assumption) $\mu_m = .3$

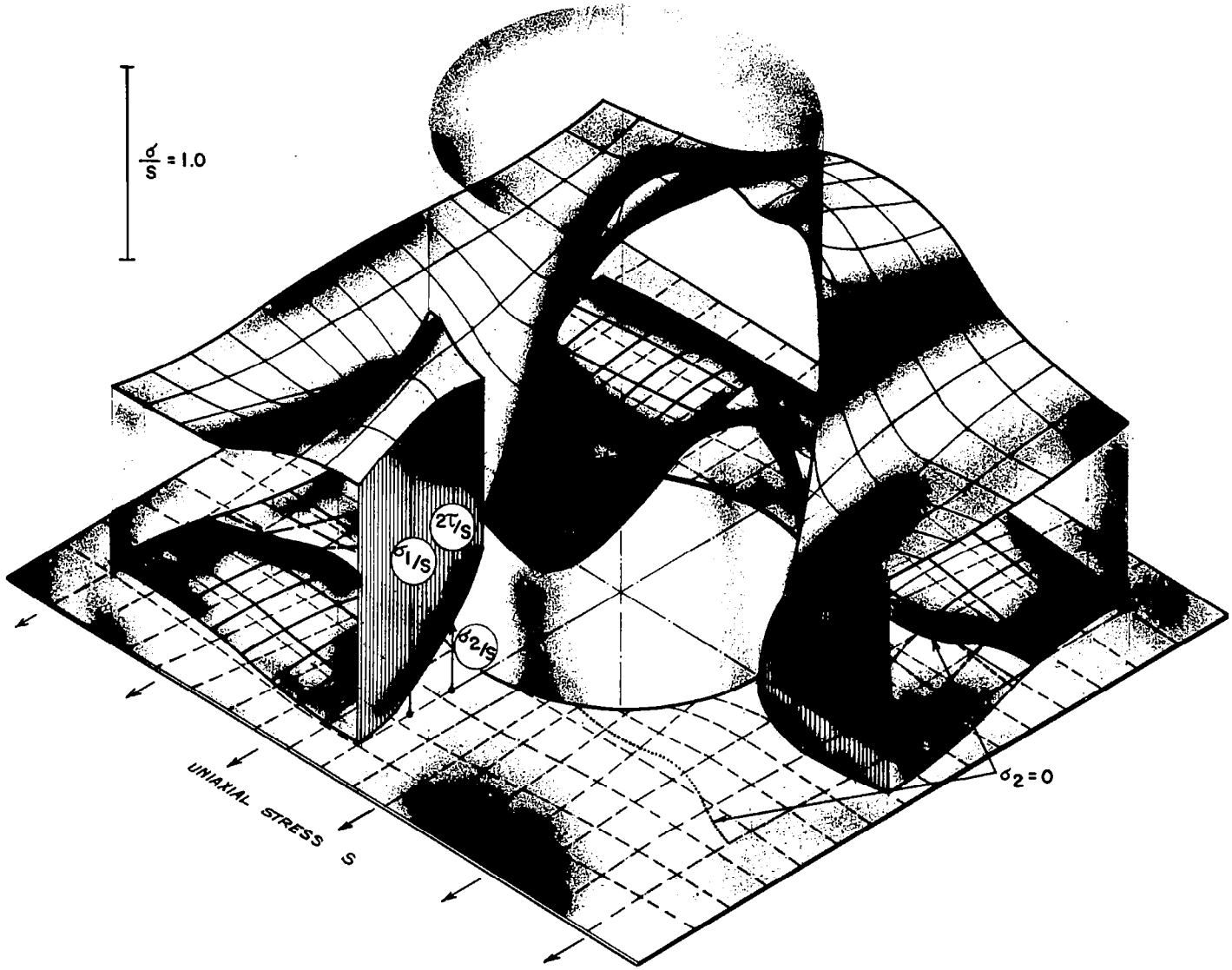

Figure 5 Stress Distribution Around A Rigid Cylindrical Inclusion (Plane Strain Assumption) $\mu_m = .3$

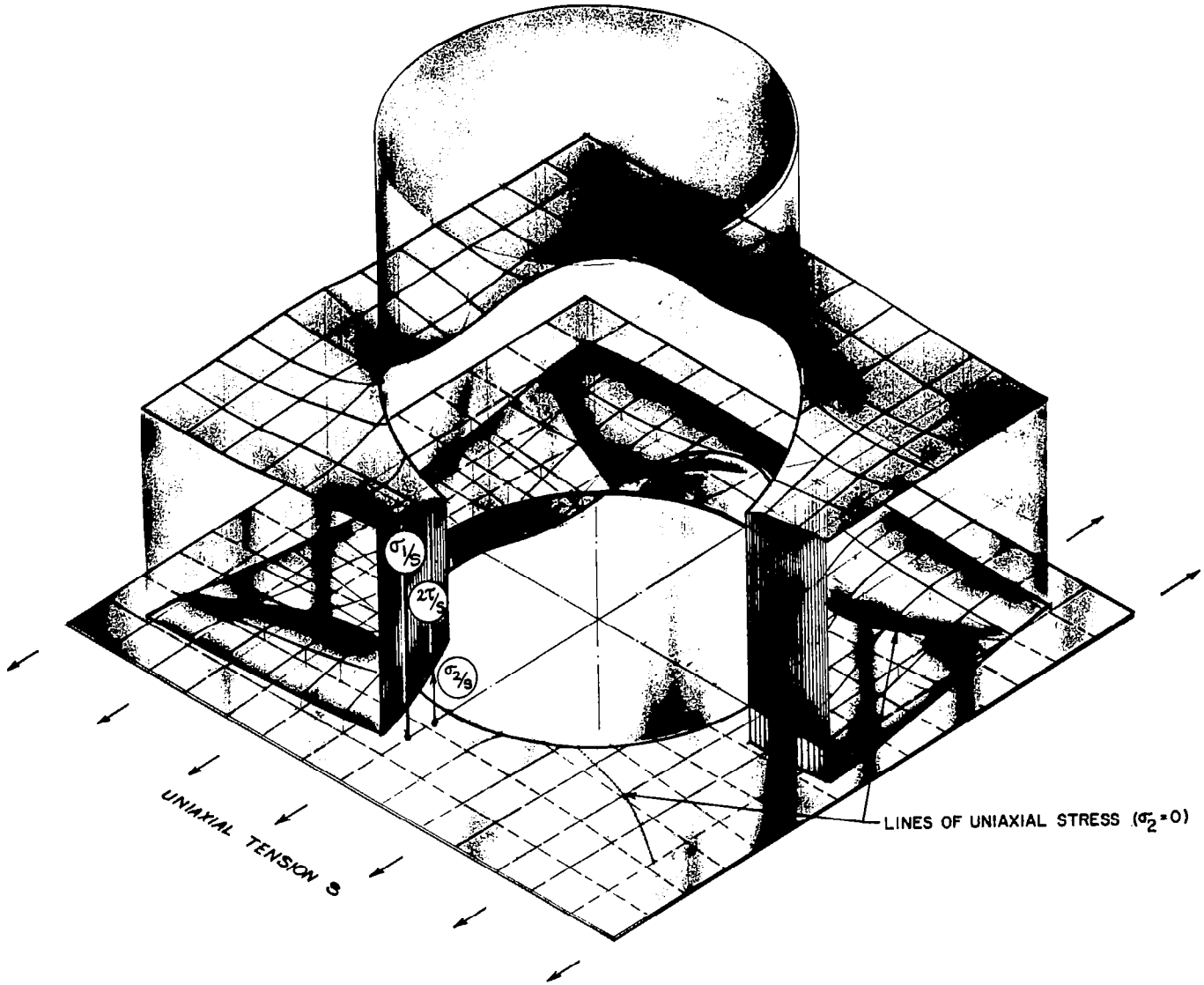

Figure 6 Stress Distribution Around A Cylindrical Inclusion With Different Poisson's Ratio (Plane Stress Assumption) $E_{f/E_m} = 1$, $\mu_f = 0$, $\mu_m = .5$

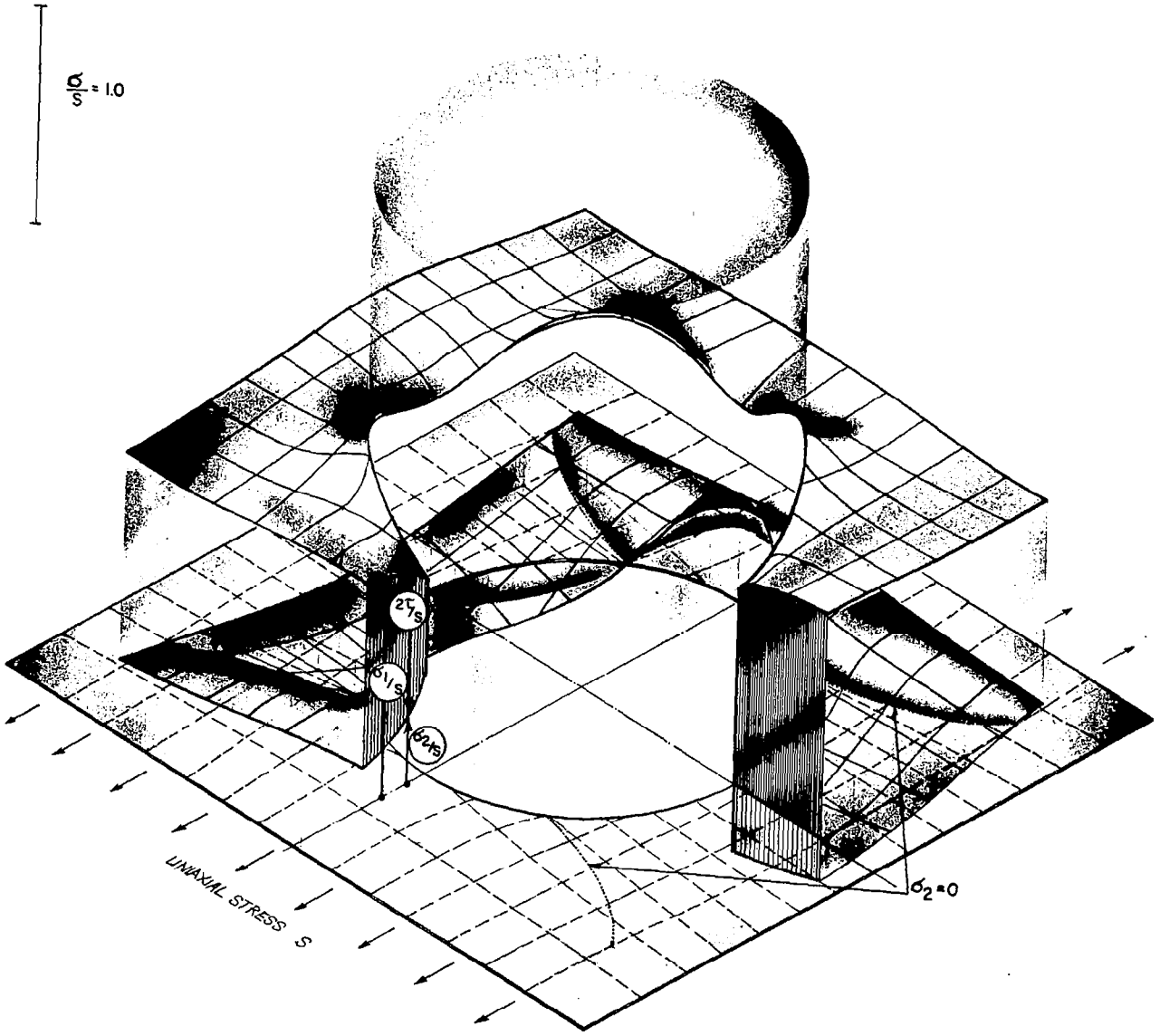

Figure 7 Stress Distribution Around A Cylindrical Inclusion With Different Poisson's Ratio (Plane Strain Assumption) $E_{f/E_m} = 1$, $\mu_f = 0$, $\mu_m = .5$

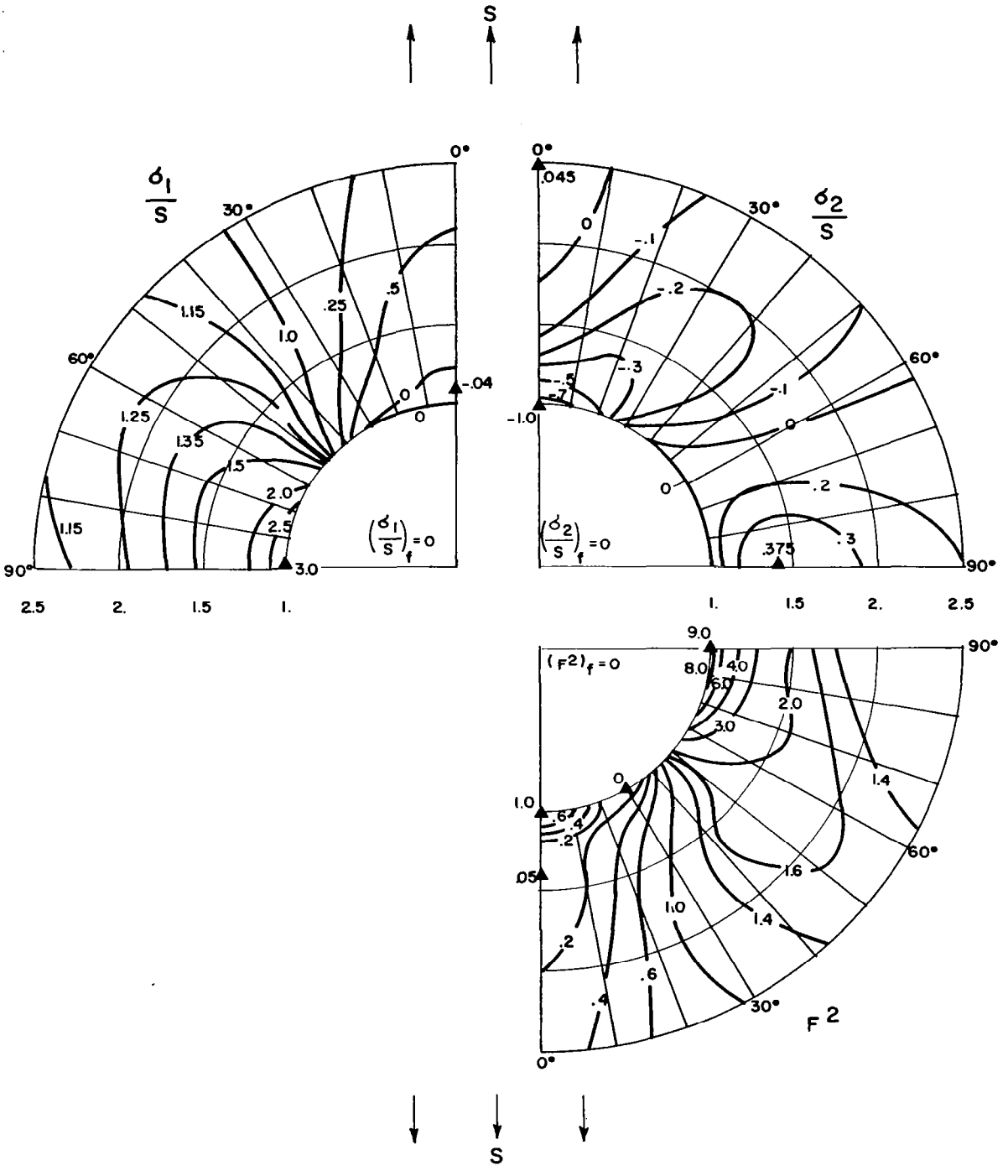

Figure 8 Stress Distribution Around A Cylindrical Void (Plane Stress Assumption) $\mu_m = .3$

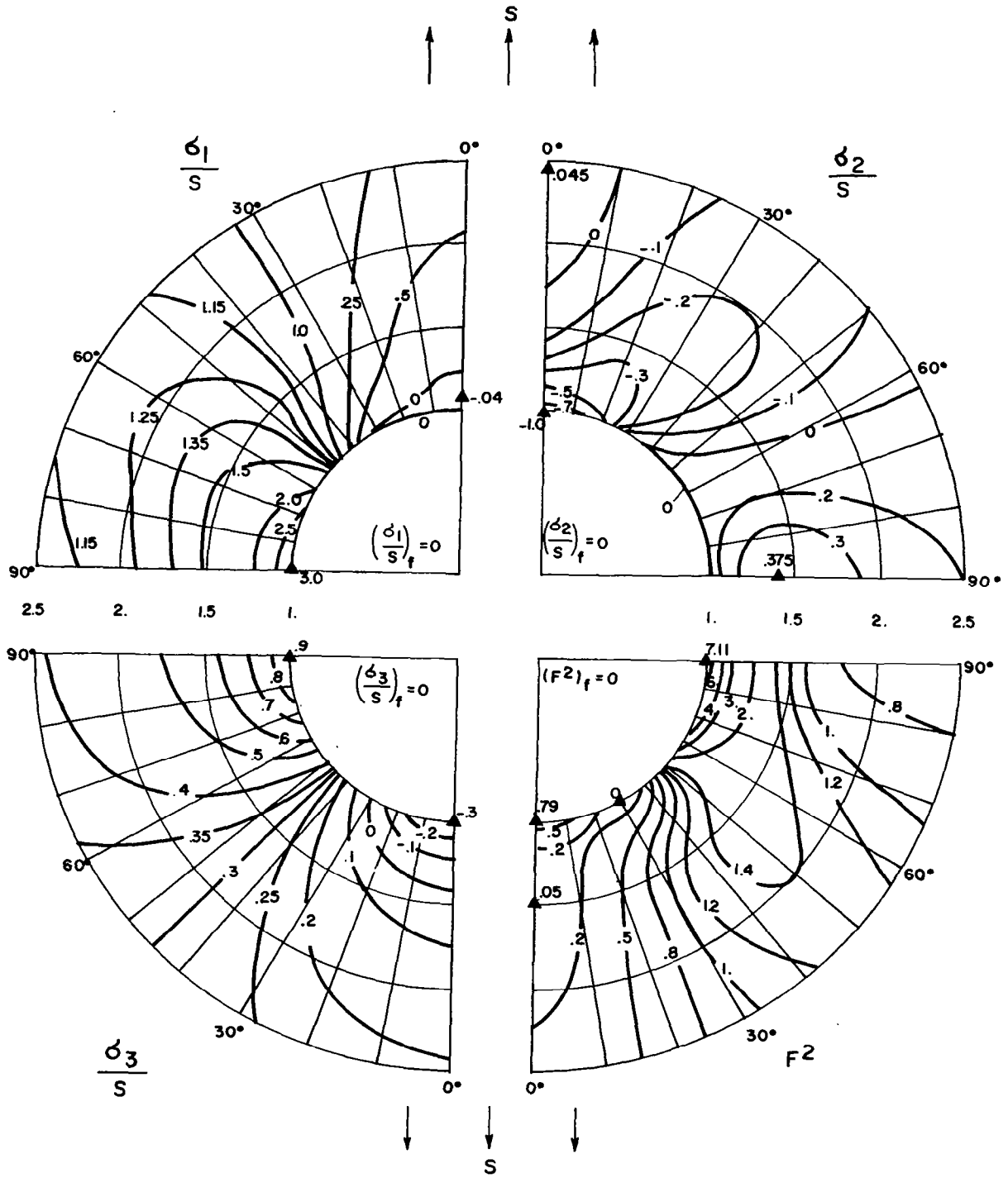

Figure 9 Stress Distribution Around A Cylindrical Void (Plane Strair Assumption) $\mu_m = .3$

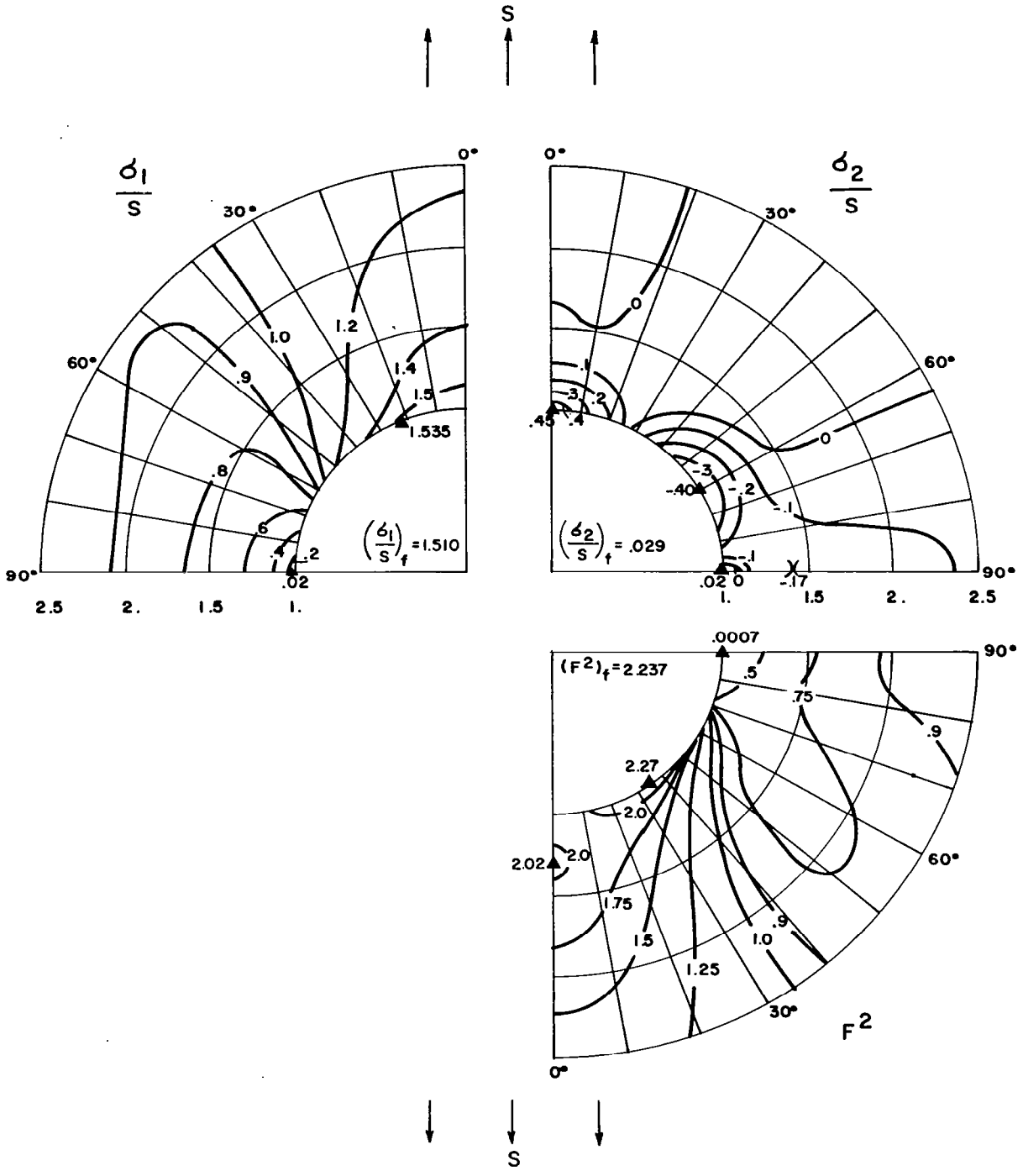

Figure 10 Stress Distribution Around A Rigid Cylindrical Inclusion (Plane Stress Assumption) $\mu_m = .3$

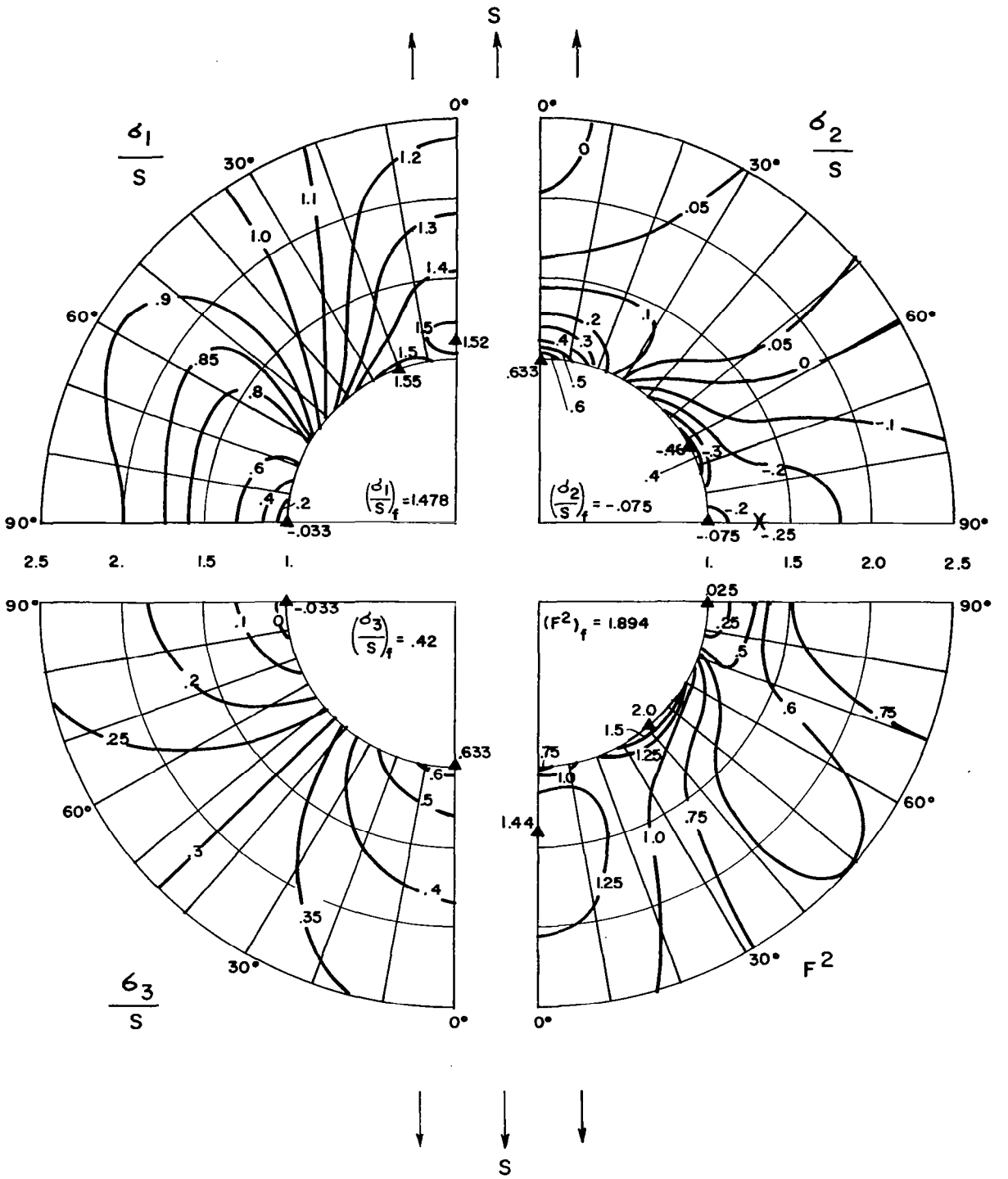

Figure 11 Stress Distribution Around A Rigid Cylindrical Inclusion (Plane Strain Assumption) $\mu_m = .3$

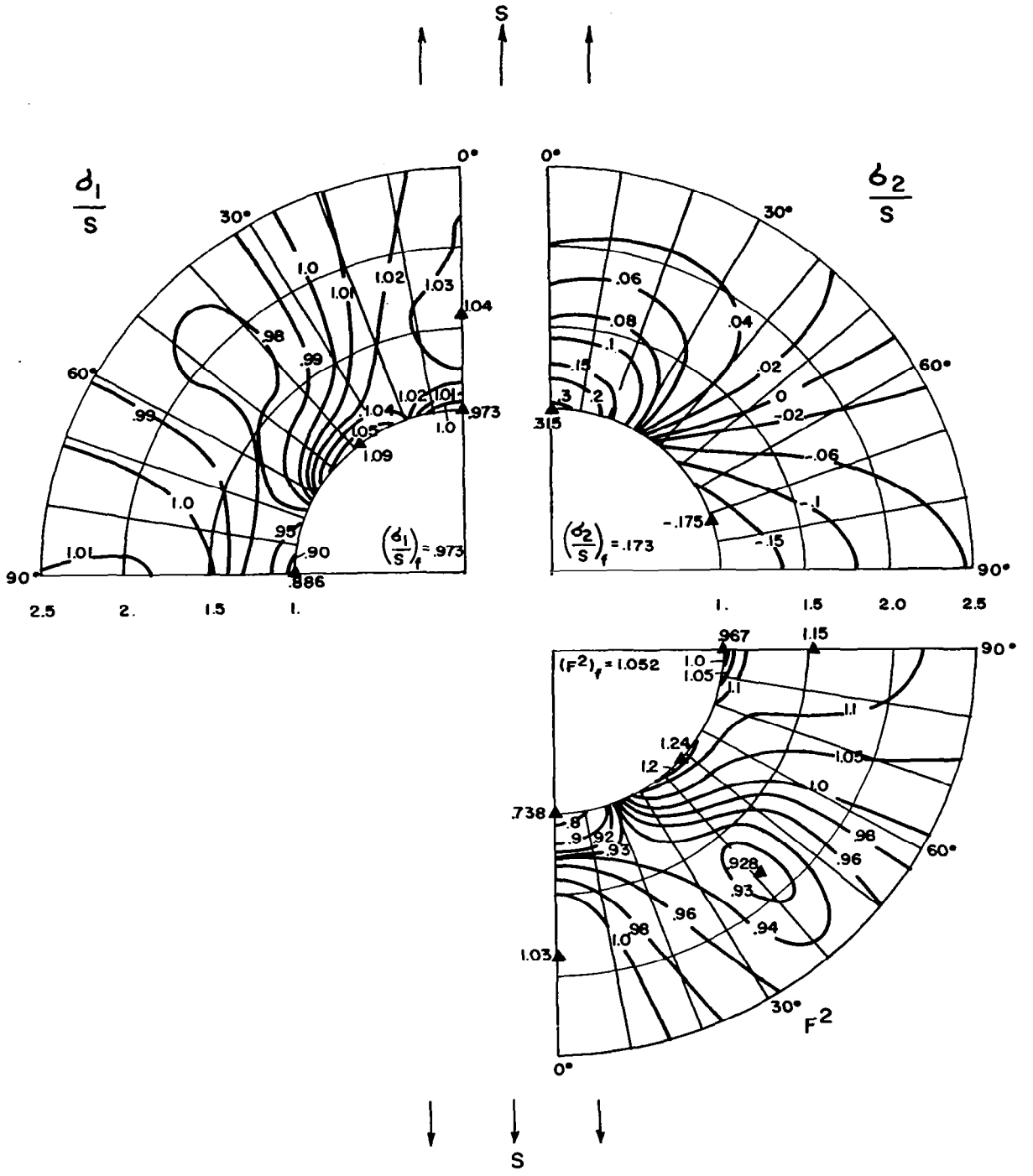

Figure 12 Stress Distribution Around A Cylindrical Inclusion With Different Poisson's Ratio (Plane Stress Assumption) $\mu_f = 0$, $\mu_m = .5$

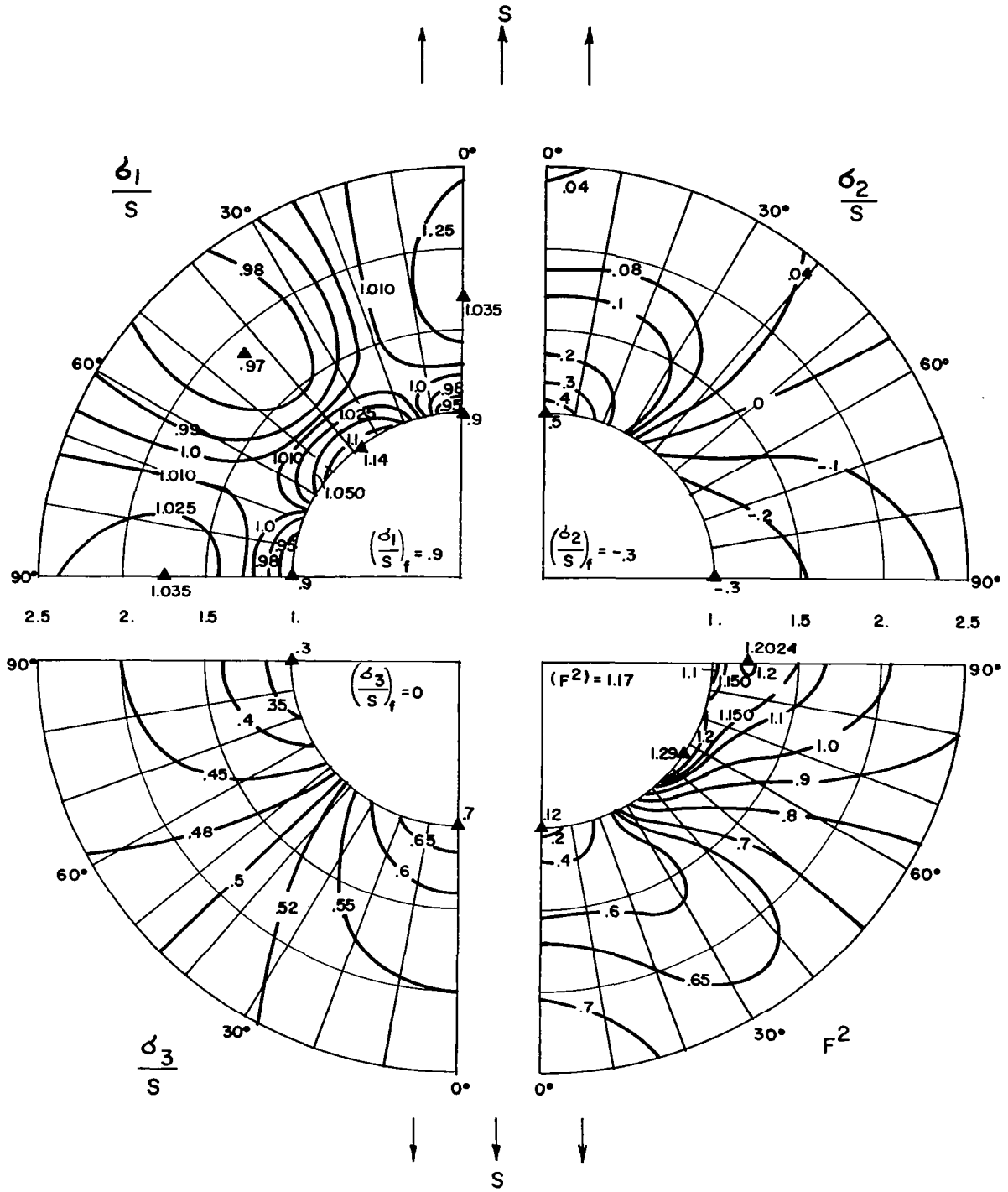

Figure 13 Stress Distribution Around A Cylindrical Inclusion With Different Poisson's Ratio (Plane Strain Assumption) $\mu_f = 0$, $\mu_m = .5$

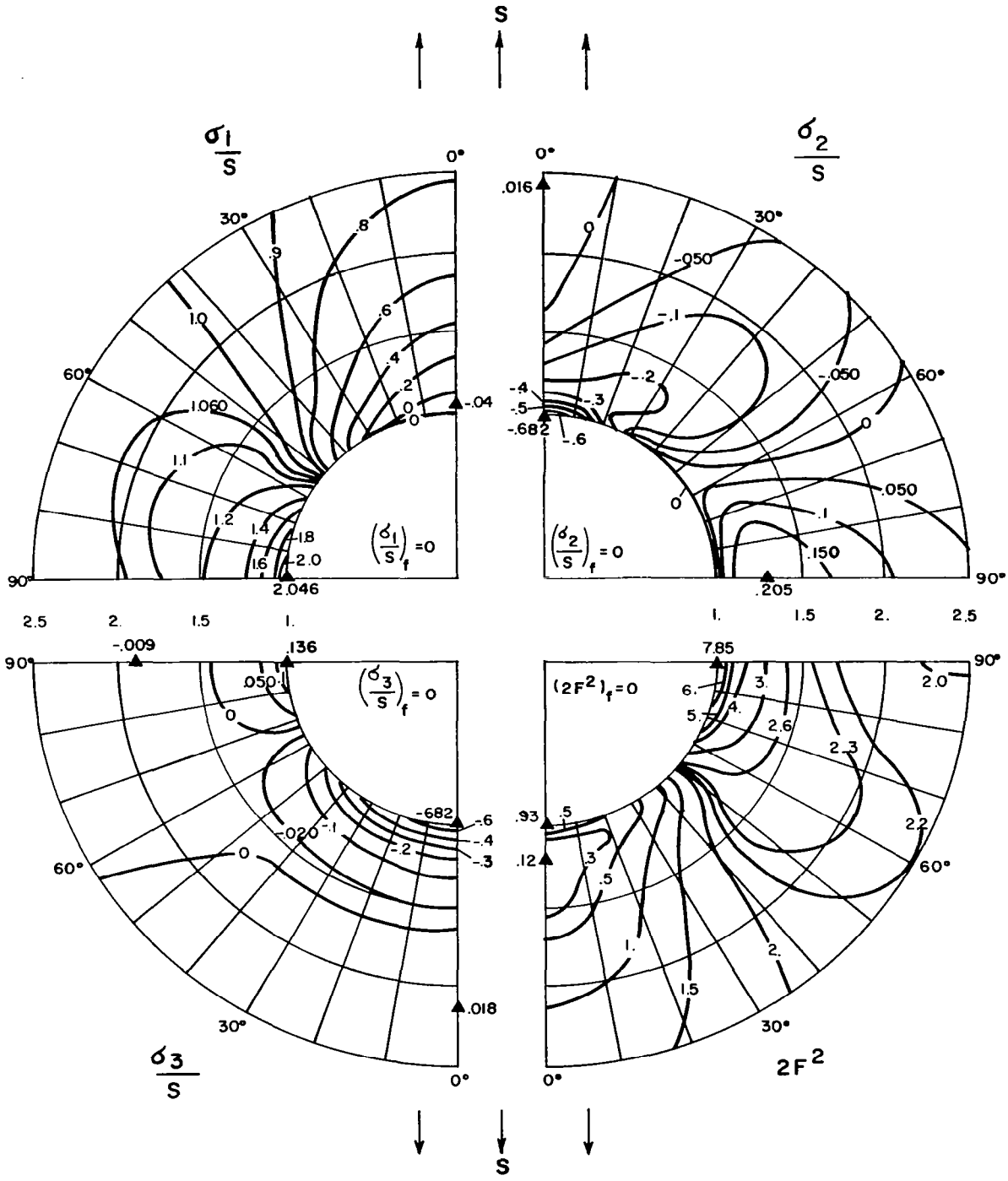

Figure 14 Stress Distribution Around A Spherical Void, Meridional Plane, μ_m = .3

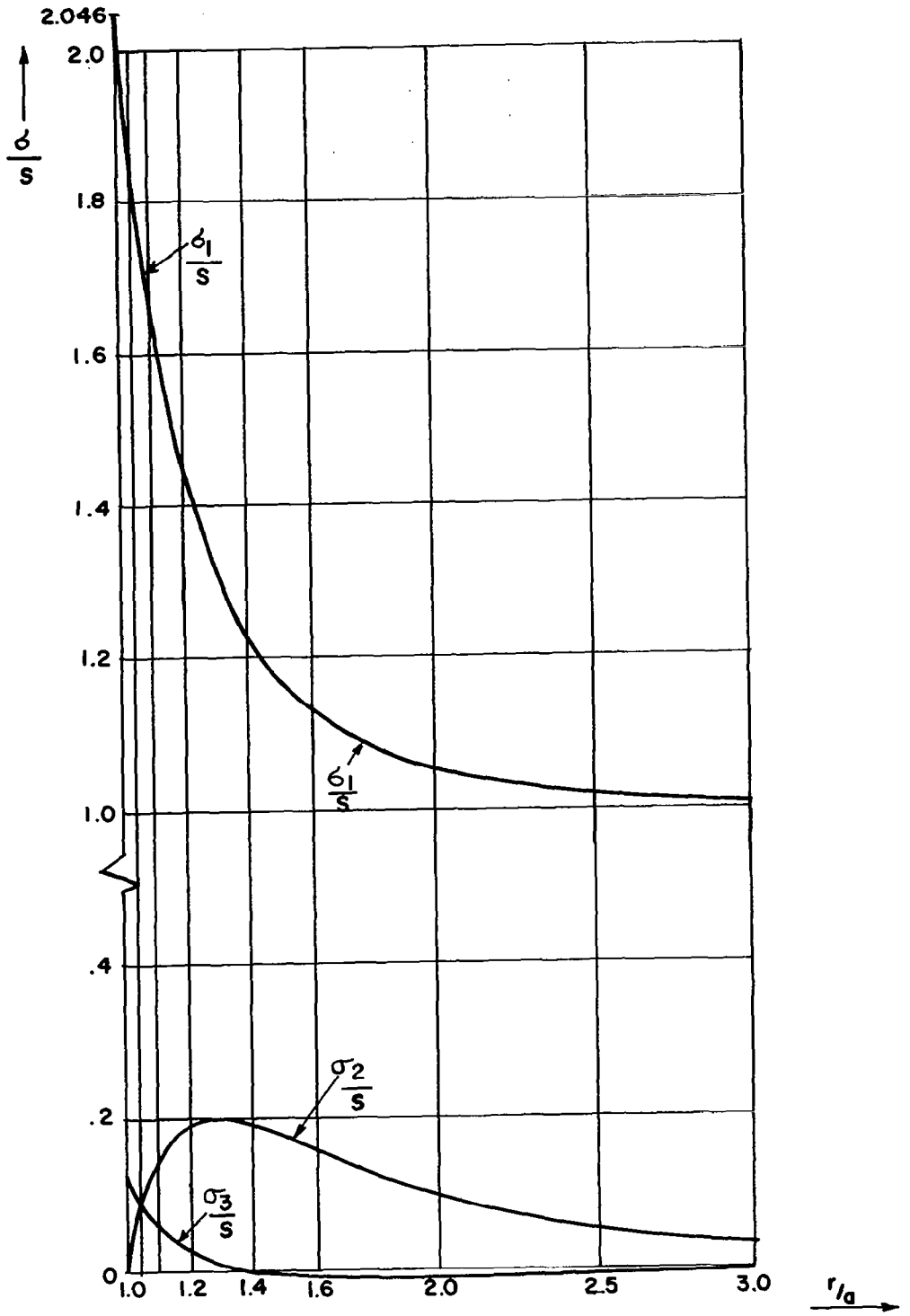

Figure 15 Stress Distribution Around A Spherical Void
Equatorial Plane $\mu_m = .3$

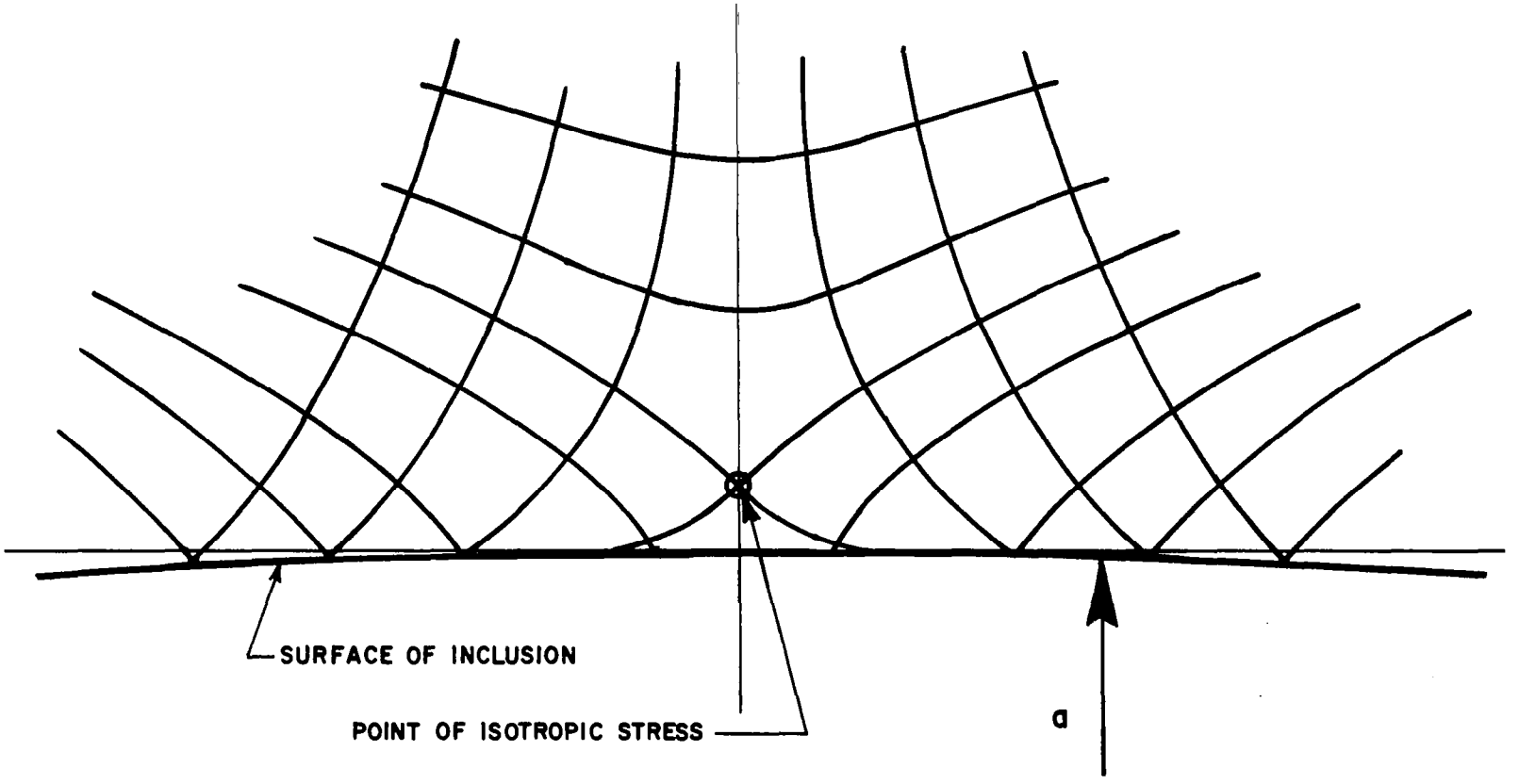

Figure 16 Singularity of Principal Stress Trajectories in Vicinity of Inclusion Surface

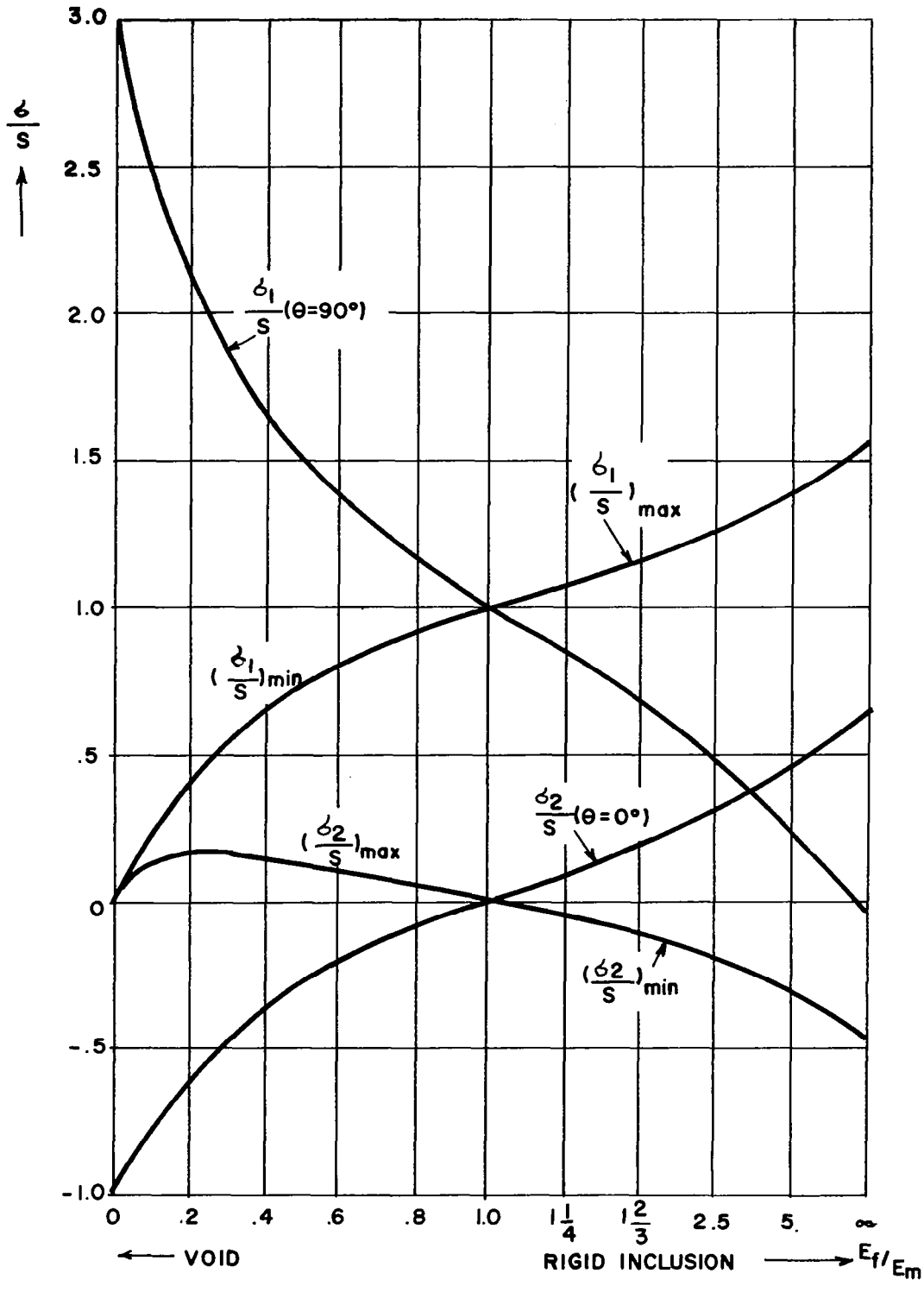

Figure 17 Magnitude of Extreme Principal Stress At Interface (Plane Strain Assumption, $\mu_f - \mu_m = .3$)

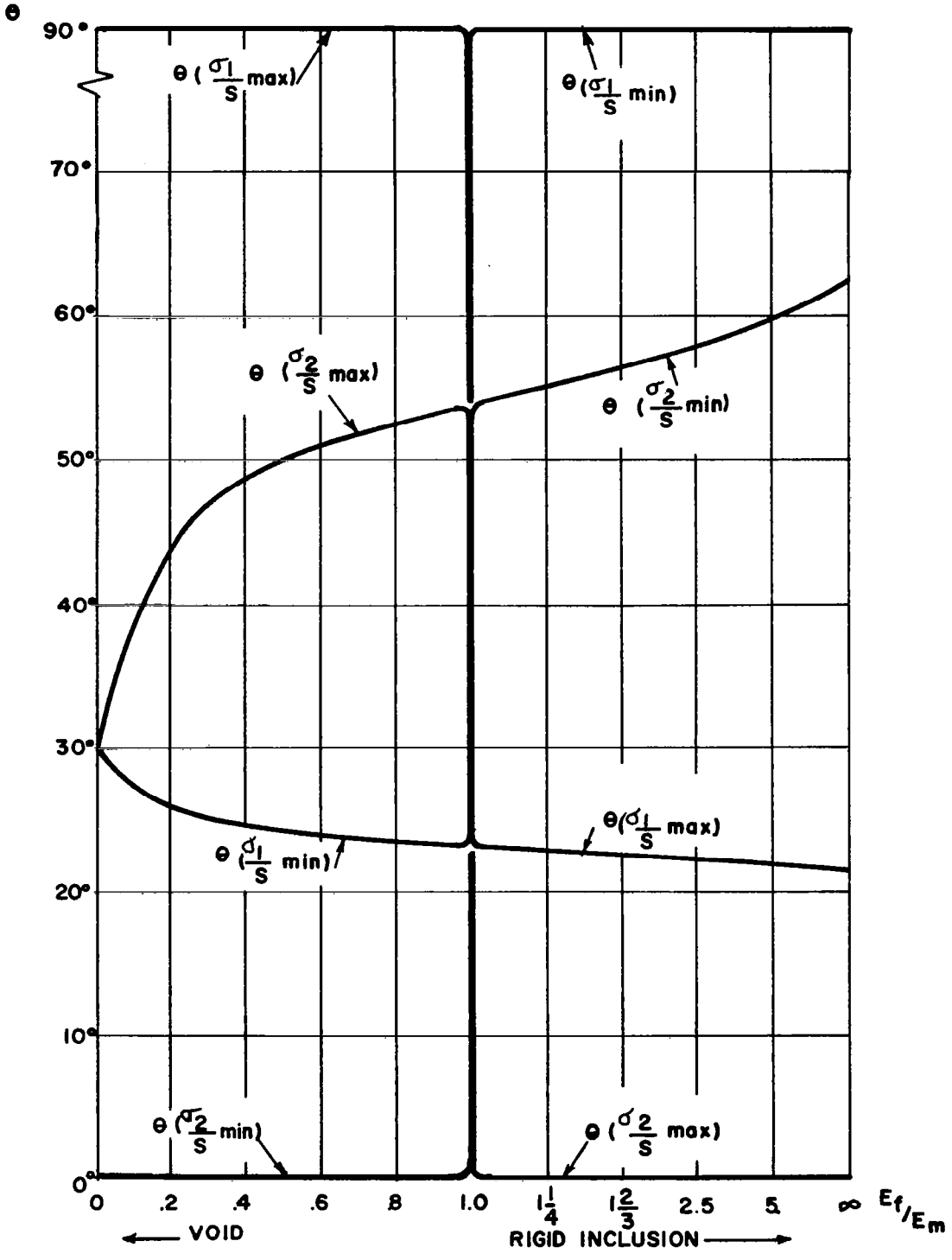

Figure 18 Location of Extreme Principal Stress At Interface (Plane Strain Assumption, $\mu_f - \mu_m = .3$)

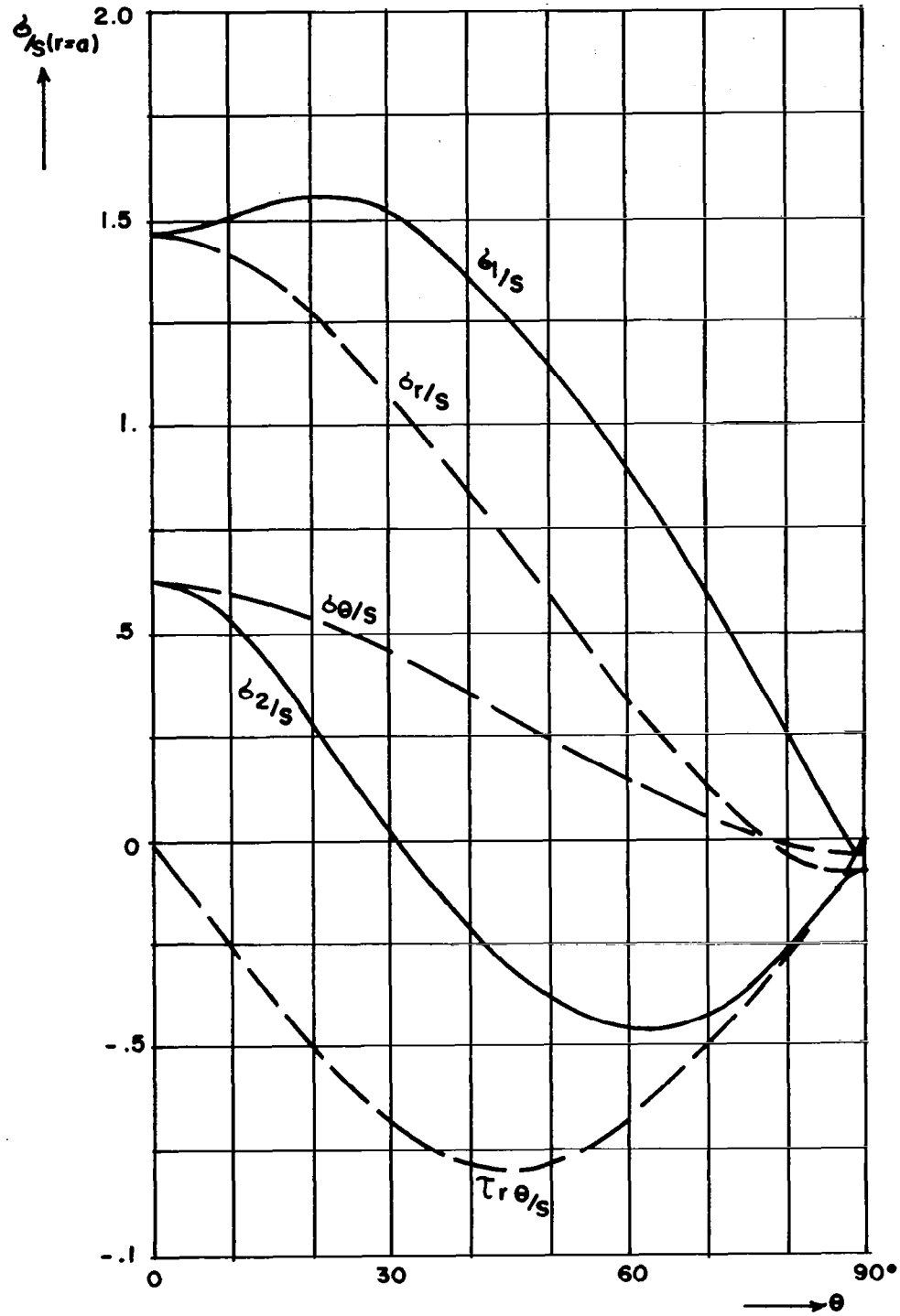

Figure 19 Stresses at Interface of Rigid Cylindrical Inclusion (Plane Strain Assumption)

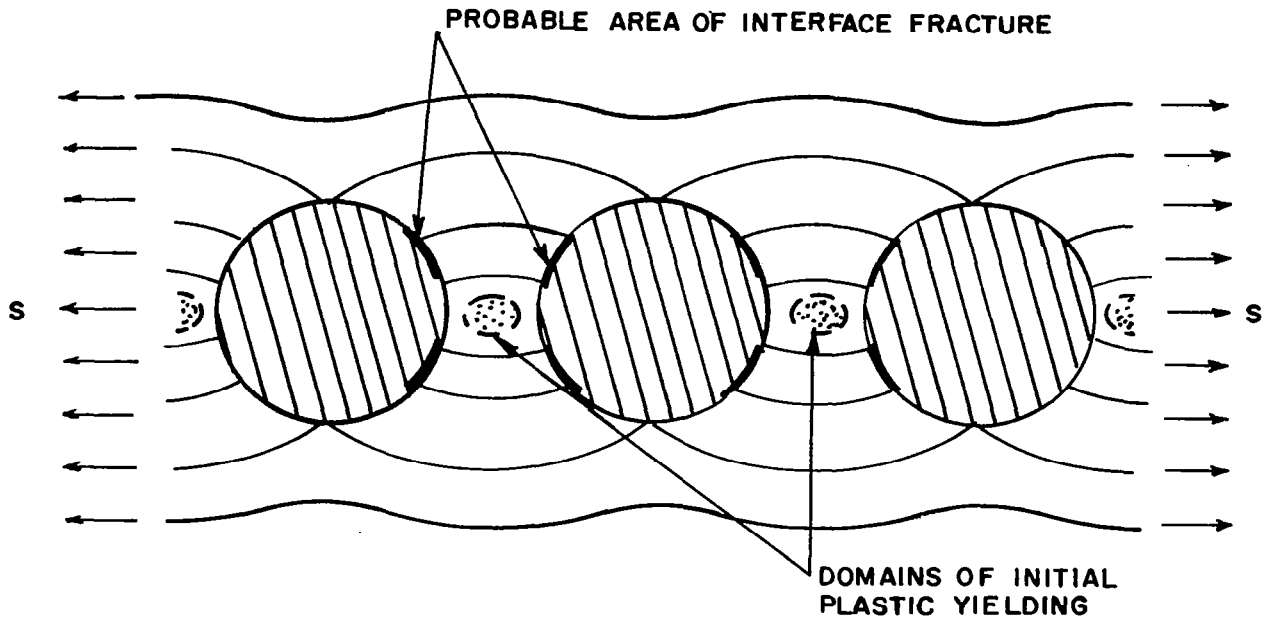

Figure 20a Array of Hard Inclusion Exhibiting "Series Failure Mode" - Plastic Yield Aggravates Stress in Critical Failure Area

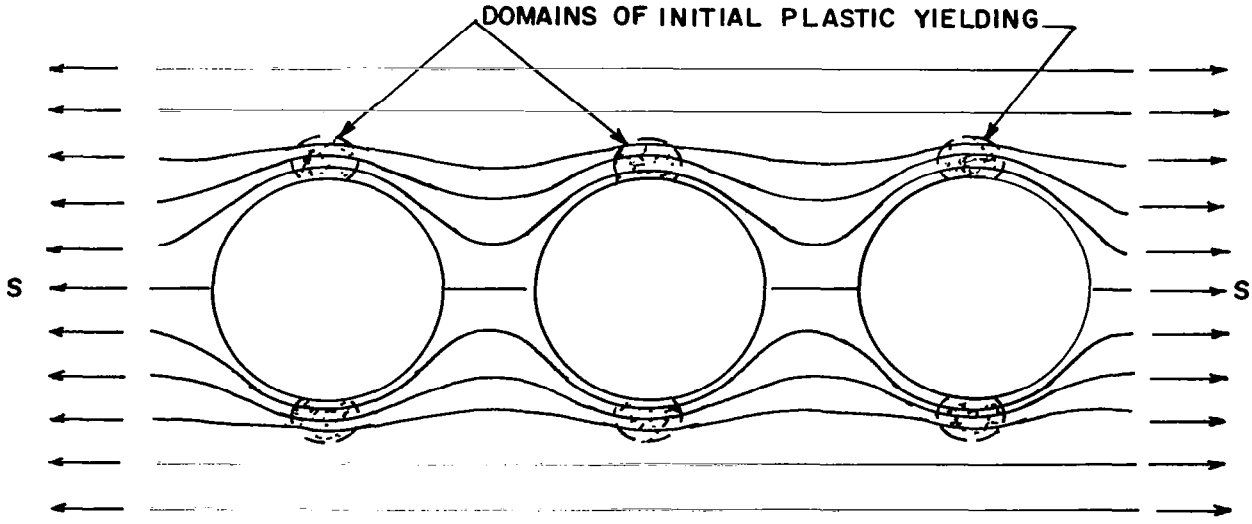

Figure 20b Array of Voids Exhibiting Parallel Failure Mode - Ductile Stress Relief

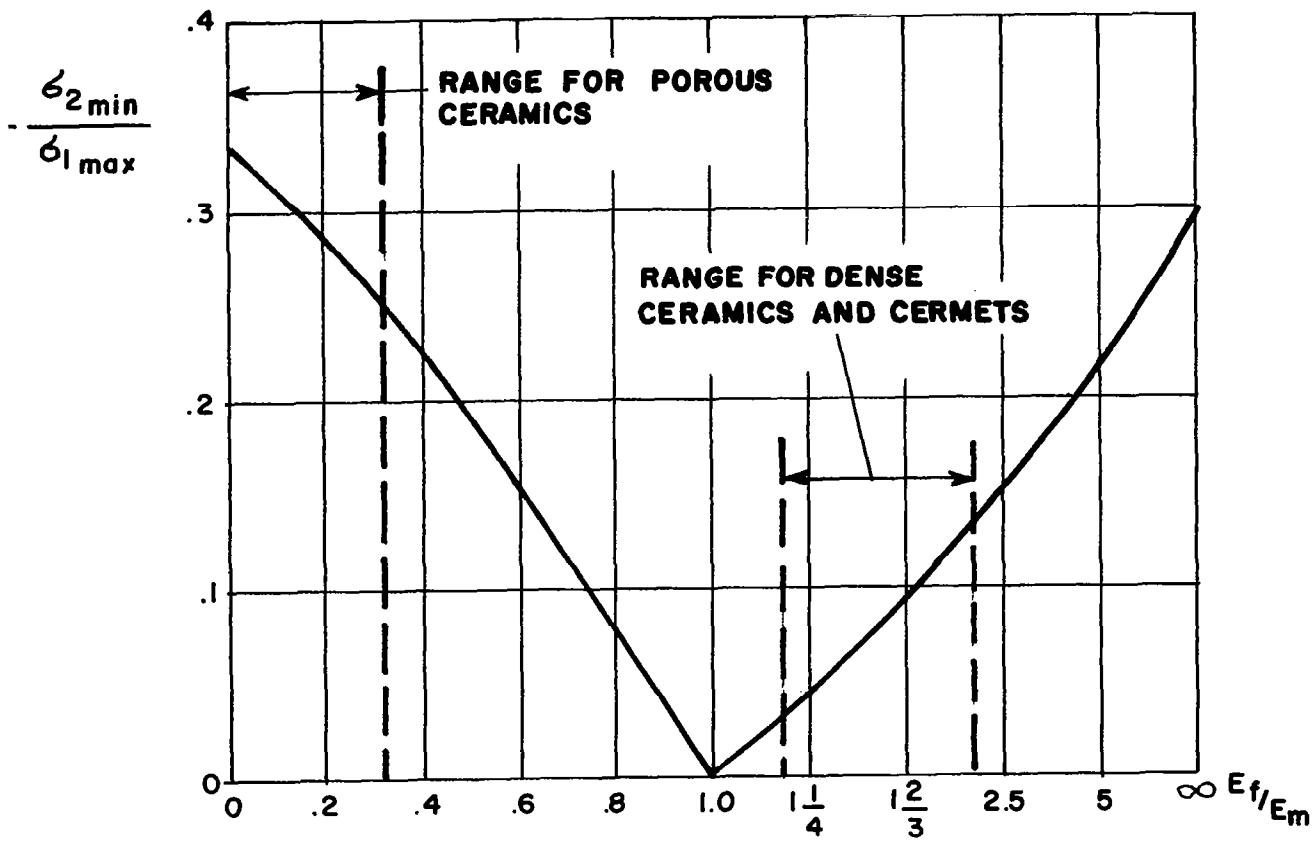

Figure 21 Ratio of Stress Concentration Extremes

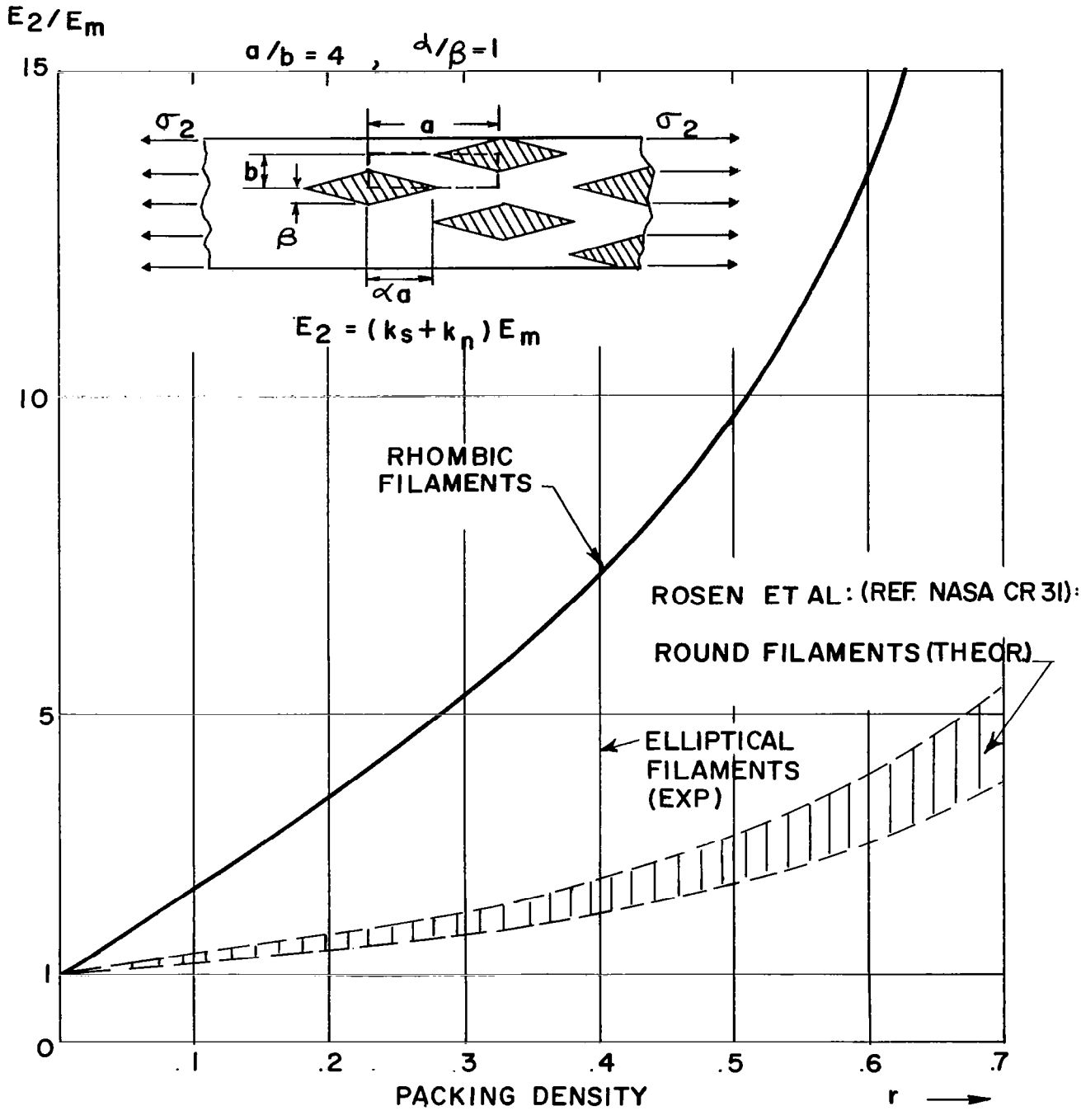

Figure 22 Transverse Modulus, E_2, of Composites With Round, Elliptical and Rhombic Fiber Sections

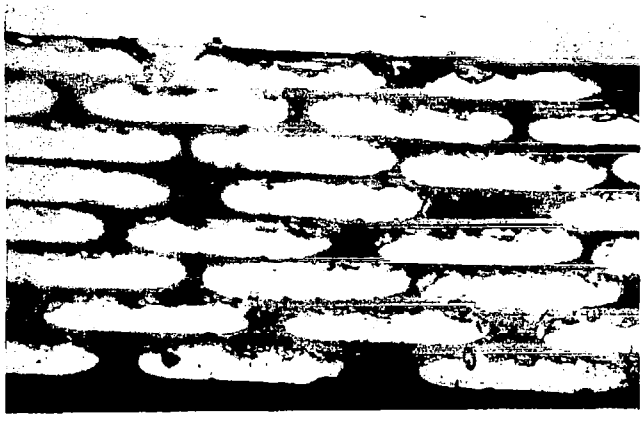

Figure 23 Composite Made From Fiber With Quasi-Elliptical Section

Figure 24 Two-stage Composite With Rhombic Tape Reinforcement

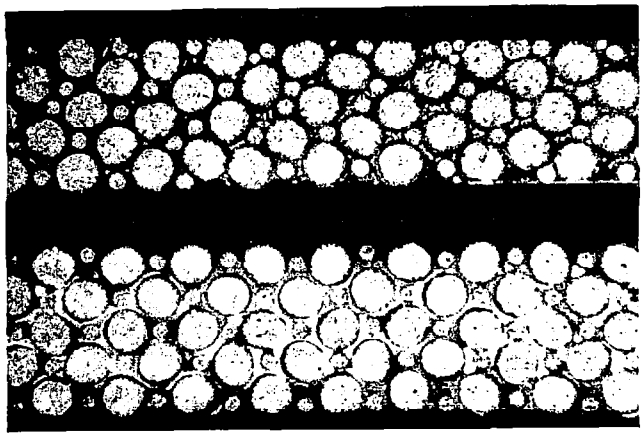

Figure 25 Two-stage Composites With Aggregate Fiber Diameters

Figure 26 Cross-woven Mat of Graded Fiberglass Rods Prior to Lamination

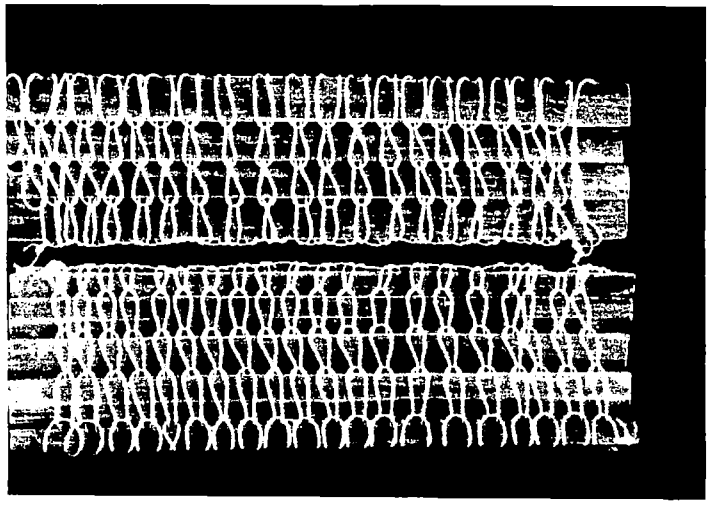

Figure 27 Cross-woven Mat of Rhombic Fiberglass Tape Prior to Lamination

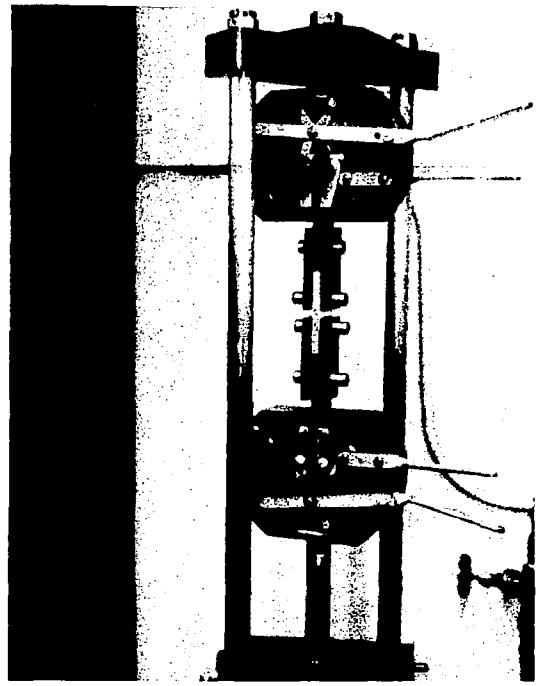

Figure 28 Shear-Bearing Test Fixture

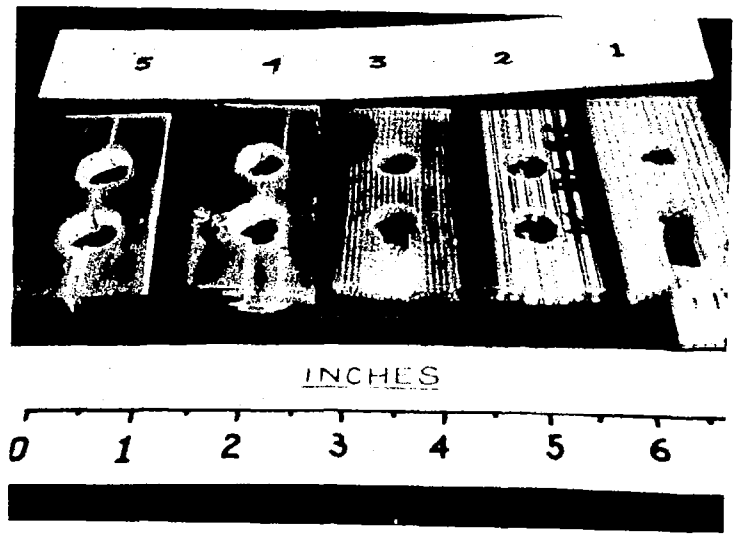

Figure 29 Fracture-Type of 5 Shear-Bearing Joint Test Specimens

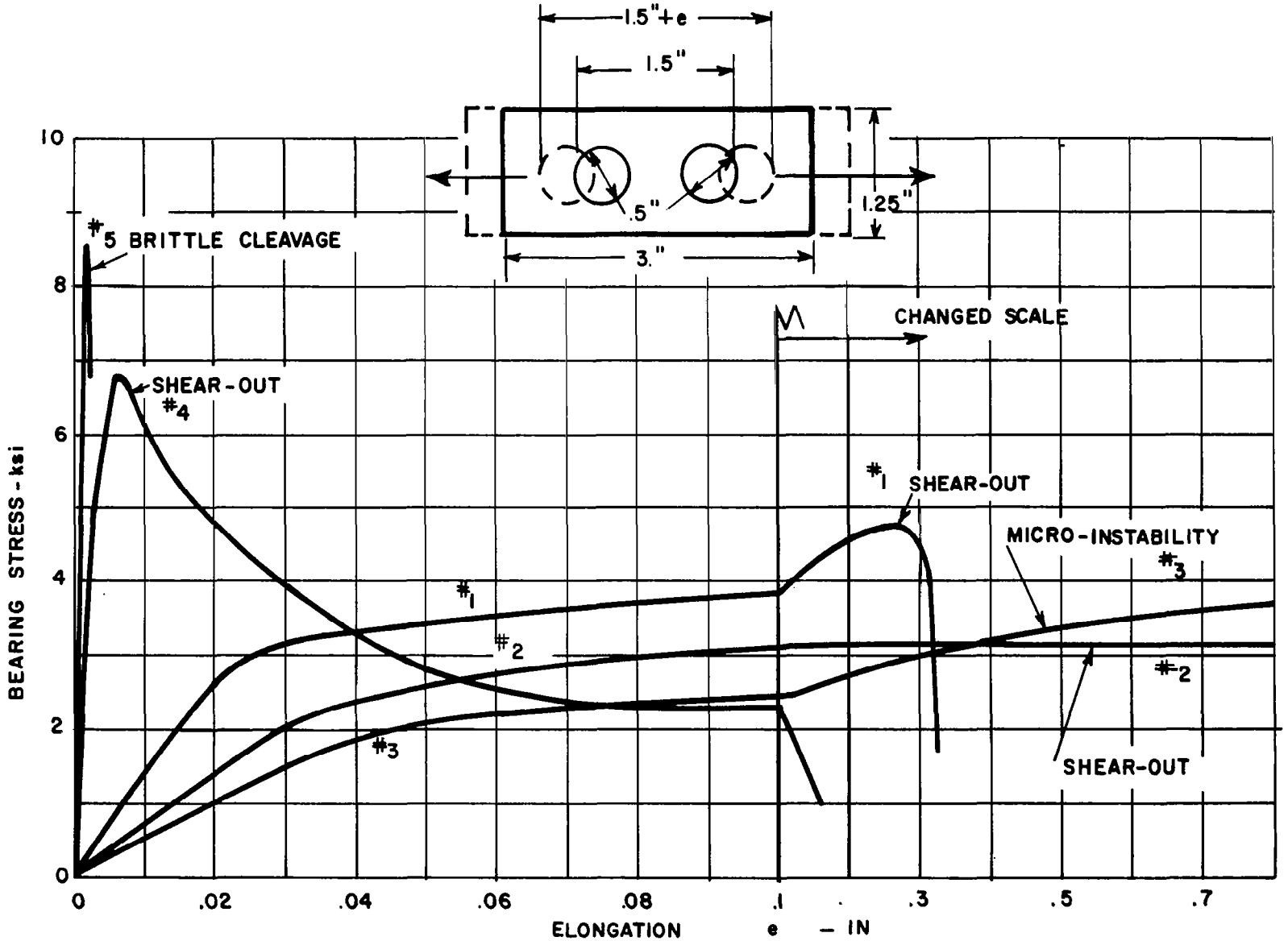

Figure 30 Bearing Stress Vs Elongation

"The aeronautical and space activities of the United States shall be conducted so as to contribute . . . to the expansion of human knowledge of phenomena in the atmosphere and space. The Administration shall provide for the widest practicable and appropriate dissemination of information concerning its activities and the results thereof."

—NATIONAL AERONAUTICS AND SPACE ACT OF 1958

NASA SCIENTIFIC AND TECHNICAL PUBLICATIONS

TECHNICAL REPORTS: Scientific and technical information considered important, complete, and a lasting contribution to existing knowledge.

TECHNICAL NOTES: Information less broad in scope but nevertheless of importance as a contribution to existing knowledge.

TECHNICAL MEMORANDUMS: Information receiving limited distribution because of preliminary data, security classification, or other reasons.

CONTRACTOR REPORTS: Technical information generated in connection with a NASA contract or grant and released under NASA auspices.

TECHNICAL TRANSLATIONS: Information published in a foreign language considered to merit NASA distribution in English.

TECHNICAL REPRINTS: Information derived from NASA activities and initially published in the form of journal articles.

SPECIAL PUBLICATIONS: Information derived from or of value to NASA activities but not necessarily reporting the results of individual NASA-programmed scientific efforts. Publications include conference proceedings, monographs, data compilations, handbooks, sourcebooks, and special bibliographies.

Details on the availability of these publications may be obtained from:

SCIENTIFIC AND TECHNICAL INFORMATION DIVISION

NATIONAL AERONAUTICS AND SPACE ADMINISTRATION

Washington, D.C. 20546